Forearc basin stratigraphy resulting from syntectonic sedimentation during accretionary wedge growth: Insights from sandbox analogue experiments

Atsushi Noda[1], Hiroaki Koge[2*], Yasuhiro Yamada[3], Ayumu Miyakawa[1], and Juichiro Ashi[2]

[1]Geological Survey of Japan, National Institute of Advanced Industrial Science and Technology (AIST), Central 7, Higashi 1-1-1, Tsukuba, Ibaraki 305-8567, Japan

[2]Atmosphere and Ocean Research Institute, The University of Tokyo, 5-1-5 Kashiwanoha, Kashiwa-shi, Chiba 277-8564, Japan

[3]Japan Agency for Marine-Earth Science and Technology (JAMSTEC), 3173-25 Showa-machi, Kanazawa, Yokohama 236-0001, Japan

Key Points:

- Sandbox analogue experiments were performed to examine forearc basin stratigraphy deposited on a growing accretionary wedge.
- Syntectonic sedimentation stabilized the inner wedge and each successive forethrust was active for long in the outer wedge.
- Changes in the stress state within and at the base of the wedge due to sedimentation may modify the deformation pattern of the wedge.

*Current address, Geological Survey of Japan, National Institute of Advanced Industrial Science and Technology, Central 7, Higashi 1-1-1, Tsukuba, Ibaraki, Japan

Corresponding author: Atsushi Noda, a.noda@aist.go.jp

Abstract

Forearc basin stratigraphy is expected to record a detailed history of the deformation and growth pattern of an accretionary wedge. However, the relationship between syntectonic basin sedimentation and growth of a wedge remains poorly understood, including (1) how deformation of the wedge modifies the basin stratigraphy and (2) how syntectonic sedimentation influences deformation of the wedge. In this study, we conducted scaled analogue sandbox experiments to reproduce accretionary wedges with and without syntectonic sedimentation. The results show that basin stratigraphy varied with the growth pattern of the accretionary wedge. In the case that wedge growth was dominated by trenchward accretion, the depositional area migrated landward. In contrast, prolonged underthrusting caused the sediment layers to be tilted landward and the depocenter to migrate landward. The occurrence of two types of basin stratigraphy (i.e., trenchward and landward migration of the depocenter) reflects a contrast in strength of the basal shear resistance between the inner and outer parts of the wedge due to sedimentation on the wedge. A change in the magnitude of normal stress acting on the wedge base likely influenced the mode of deformation of the wedge. A phase dominated by underthrusting can result in the combining a retro-wedge basin with a wedge-top basin, and yield a wide area of accommodation space in the forearc basin. These results suggest that forearc basin stratigraphy is influenced by the growth pattern of an accretionary wedge that is affected by syntectonic sedimentation.

1 Introduction

The formation of a forearc basin at an accretionary margin is controlled by deformation of the accretionary wedge, which depends on various factors including the material properties of the wedge and the décollement (friction, cohesion, and pore fluid pressure), plate convergence (obliquity and velocity), isostatic response (uplift and subsidence), and external surface processes (erosion and sedimentation) (e.g., Byrne et al., 1988; Malavieille et al., 1993; Wang & Davis, 1996; Gutscher et al., 1998; Fuller et al., 2006; Graveleau & Dominguez, 2008; Simpson, 2010; Mannu et al., 2017; Noda, 2016, 2018). Among these factors, external surface processes can strongly influence deformation of the accretionary wedge (e.g., Storti & McClay, 1995; Simpson, 2010; Cruz et al., 2011) by (1) concentrating deformation at the

rear of the wedge (Storti & McClay, 1995; Hardy et al., 1998), (2) reducing the taper angle (Storti & McClay, 1995; Bigi et al., 2010; Simpson, 2010), (3) decreasing the number of thrusts and widening the thrust spacing, which is likely caused by a reduction in differential stress in the wedge due to an increase in normal stress (Liu et al., 1992; Bigi et al., 2010; Simpson, 2010; Fillon, Huismans, & van der Beek, 2013; Zhang et al., 2019), (4) increasing the duration of folding at the upper ramp tip (Storti et al., 1997), (5) prolonging the phase of underthrusting and limiting the forward propagation of thrust activity (Hardy et al., 1998; Del Castello et al., 2004), (6) forming a trishear zone and causing limb rotation (Wu & McClay, 2011), (7) creating and reactivating out-of-sequence thrusts (Storti et al., 2000; Mannu et al., 2016), (8) stabilizing the rear of the wedge and increasing the rate of migration of the deformation front (Fillon, Huismans, & van der Beek, 2013), and (9) causing a switch from frontal accretion to synchronous thrusting and underthrusting due to local heterogeneity of the basal shear stress (Storti et al., 2000; Del Castello et al., 2004; Bigi et al., 2010).

Forearc basin stratigraphy deposited on a deforming accretionary wedge is expected to record a dynamic history of accretionary wedge growth in response to the syntectonic sedimentation processes listed above. Stratigraphic records of forearc basins, established from high-resolution seismic and deep-sea drilling core data, can be used to understand the factors controlling sedimentation at subduction margins (e.g., Moore et al., 2015). However, it can be difficult to unravel time-series evolving relation between sedimentation in the basin and deformation of the wedge from only field data. For this reason, forward modelling approaches, such as sandbox analogue experiments, have been widely used to understand the mechanisms controlling the dynamics and evolution of fold-and-thrust belts, accretionary wedges, and forearc basins (e.g., Graveleau et al., 2012).

Few studies have performed analogue experiments with a focus on forearc basin stratigraphy (Malavieille et al., 1993; Larroque et al., 1995). These studies found that contraction and thickening of the retro-wedge of the accretionary body, associated with backthrusts, allowed forearc basins to form. In addition, filling patterns in forearc basins are influenced by the deformation style of the wedge, which in turn is related to basal friction. However, these pioneering studies did not control the sediment input and assumed that the forearc basin was always overfilled

regardless of how much accommodation space was created, with sediment supply being one of the key controls on the wedge growth pattern and basin stratigraphy (Noda, 2018). From a technical standpoint, the step-by-step shortening adopted by these studies has the potential to change the frictional properties of active thrusts from dynamic to static (c.f., Klinkmüller et al., 2016).

The purpose of this study is to investigate how deformation processes in an accretionary wedge modify basin stratigraphy and how syntectonic sedimentation influences the deformation pattern in the wedge. We performed sandbox analogue experiments, focusing on controlling the sediment input with continuous shortening. We examined the geometrical characteristics of the wedge, thrust activity, stratigraphic patterns, and the state of stress of the wedge for cases with and without syntectonic sedimentation.

2 Materials and Methods

2.1 Experimental Materials

In our experiments, we used a scaled two-dimensional analogue modelling technique to allow results to be compared with naturally occurring geological structures (e.g., Buiter, 2012; Graveleau et al., 2012). The scaled sandbox experiments are based mainly on the Mohr-Coulomb behaviour of materials used for the input sediment and growing wedge. Major factors controlling the shape of the wedge, which is made of dry cohesionless particles, include the slope of the wedge surface, the dip of the subducting plate, the internal friction of the wedge material, and basal friction along the décollement (Davis et al., 1983; Dahlen, 1984). Dry granular materials, such as quartz sand, display elastic–frictional plastic behaviour and reproduce the non-linear deformation behaviour of brittle crustal rocks. For this reason, such materials are widely used as analogue materials to simulate the brittle and frictional behaviour of sedimentary rocks in an accretionary wedge (e.g., Dahlen, 1984; Lohrmann et al., 2003; Graveleau et al., 2012).

We used two types of granular material, Toyoura sand and glass microbeads. Toyoura sand, a standard testing material commonly used by Japanese civil engineers, is a spherical-grained quartz-rich sand with a particle size of 0.14–0.26 mm (D_{50} = 0.2 mm), a density of approximately 1600 kg m^{-3}, an internal

coefficient of friction $\mu = 0.59$–0.68, and a cohesion $C = 105$–127 Pa (Yamada et al., 2006; Dotare et al., 2016). The glass microbeads are spherical and 0.045–0.063 mm in diameter, have a low internal coefficient of friction ($\mu_b = 0.47$) and low cohesion (40 Pa), and are considered to be a suitable analogue for weaker layers (Yamada et al., 2006, 2014).

2.2 Model Setup

The apparatus used in the experiment was a glass-sided, rectangular deformation rig with internal dimensions of 100 cm × 30 cm × 20 cm deep (Figure 1). A steel plate was positioned at one end with a small window below it. A rigid wedge made of wood was placed next to the steel plate but was not fixed to it. The wooden wedge was designed to behave like a static backstop that has a higher mechanical strength than the accretionary wedge (e.g., Tsuji et al., 2015). The rigidity of the backstop was used to ensure stability during the experiments and for repeatability. The mobility of the backstop helped to replicate the deformable nature of equivalent structures found in natural geological systems. The backstop had a dip slope of 30° with a sandpaper surface. A plastic (Mylar®) sheet was placed over the base plate of the rig and fixed to the stepper motor behind the wooden wedge (left side, Figure 1). The stepper motor was used to pull the plastic sheet beneath the rigid backstop at a rate of 0.5 cm/min, thereby compressing the material above. The total length of horizontal shortening was about 30 cm for all of the experiments.

Layers of sand and glass microbeads with a total thickness of 3.4 cm were used in the experiments (Figure 1). The sand and glass microbeads were sprinkled into the rig from a height of approximately 30 cm above the rig floor. Alternating layers of blue, red, and black sand were used to help visualize the cross-sectional geometry of the models without influencing the mechanical homogeneity of the sand. Mechanically weak layers were created by adding a thin layer (3 mm) of glass microbeads. The layers of sprinkled sand and microbeads on the basal sheet represent the deep sea sediments and trench fill overlying the subducting oceanic plate, respectively.

Experiment A1 (Exp. A1) was performed to assess how an accretionary wedge grows without syntectonic sedimentation. Three other experiments (Exp. A2, A3, and A4) were designed to examine how basin stratigraphy developed while an accretionary wedge continuously grew (Figure 2). We sifted dry sand from at least 10 cm above the surface of the accretionary wedge to fill the topographic lows that had developed after each 2 cm increment of shortening. The sprinkled sand was used to replicate sedimentation in a forearc/slope basin that occurs on the surface of an accretionary wedge. Three different series of experiments of types A2, A3, and A4 were conducted, representing constant, fluctuating, and inversely fluctuating patterns of sand input, respectively. A total of 910 g of sand was added to experiments A2–A4, measuring 569 cm^3 in volume.

Time-lapse digital images were taken at 5-s intervals using a PC-based controller. The images were later analyzed to calculate the geometry of the wedge (Figure 3) and assess thrust activity and stratigraphic patterns in the basins for Exp. A2–A4. These images were then analyzed by the digital image correlation (DIC) technique to visualize the velocity field and strain rate, and thus identify thrust activity within a deforming sand body (Adam et al., 2005). The method calculates the displacement field of the grains with a theoretical resolution of ~0.5 mm. The software used for the experiments was DaVis 8.0 StrainMaster (LaVision, 2012).

2.3 Scaling

Models used in laboratory experiments should be properly scaled so that the results can be considered true analogs of real geologic settings (e.g., Hubbert, 1937). Experiments using granular materials such as dry quartz sand have been widely used to simulate geological structures (Graveleau et al., 2012) because these materials exhibit a similar behaviour to brittle rocks that respond to elastic–frictional plastic deformation with pre-failure strain hardening and post-failure strain softening until a dynamically constant shear load is reached (e.g., Lohrmann et al., 2003).

For sedimentary rocks in an accretionary wedge with mean bulk density values of 2000–2500 kg m^{-3} and cohesion values of 5–20 MPa (Schumann et al., 2014), the length-scale ratio of the experiment ranges from approximately 3 ×

10^4 to 1×10^5, meaning that a 1 cm model layer in an experiment corresponds to 300 m to 1 km in nature. Therefore, the 3.4-cm-thick sediment layers used in this experiment are equivalent to 1–3 km of strata, which is consistent with a moderate trench-fill sediment thickness for a modern accretionary margin (Noda, 2016). The total amount of shortening from the experiments was 30–35 cm, which is equivalent to 9–35 km of displacement. Assuming a plate convergence rate of 5 cm/year, this corresponds to $1.8–7 \times 10^5$ years. A sediment supply of 910 g delivered to the topographic lows for 6×10^5 years is equivalent to a sediment budget of approximately 10^6 t/year. This calculated sediment budget is similar in magnitude to the sediment load of many mountain rivers in Japan and New Zealand (Milliman & Syvitski, 1992), with the sedimentary influx into the Kumano Basin being 50 km × 70 km × 2 km over the last 4 Myr.

2.4 Limitations

The purpose of this study is not to replicate the evolution of a specific subduction margin but instead to derive a basic geodynamic framework including general features that characterize natural forearc basins. However, some caution is necessary when comparing experimental observations with natural submarine accretionary wedges since analogue experiments are performed with a dry, homogeneous material representing the accreting sediment. Excess pore pressure within the wedge and the décollement can locally produce significant changes in material properties (Hubbert & Rubey, 1959) that cannot be incorporated into the model. In addition, analogue sandbox experiments cannot reproduce modifications in mechanical strength from high temperatures caused by diagenetic alteration in a natural forearc. The experiments do not reflect the effects of the flexural response and isostatic compensation of both the overriding and subducting plates, which would create notable differences between our models and natural examples (e.g., Schellart & Strak, 2016). The backstop is totally undeformed and fixed to the side wall, so no deformation or rotation of the backstop is possible, which can modify the geometry of the wedge and outflux of materials (Gutscher et al., 1996, 1998; Kukowski & Oncken, 2006; Albert et al., 2018). We considered syntectonic sedimentation on top of the wedge in this study, but did not simulate erosional

forcing of the surface of the wedge (Mugnier et al., 1997; Graveleau & Dominguez, 2008; Konstantinovskaya & Malavieille, 2011; Perrin et al., 2013).

3 Results

We conducted four experiments, with (Exp. A2–A4) and without sedimentation (Exp. A1). A total of 16 experiments were performed, with 2 to 9 runs conducted for each case (Figure 4). Because it is commonly difficult for analogue sandbox experiments to reproduce the exact same results every time, even under controlled boundary conditions (cf. Santimano et al., 2015), our results also showed some degree of reproducibility (Figure 4).

For these experiments, we analyzed the geometry of the wedge, thrust activity, and basin stratigraphy. The time-series images of digital photographs, DIC data, and associated movies used for the analyses can be found in the data repository (Noda et al., 2019). Based on the intervals and displacement of the forethrusts, the growth pattern of the wedges occurred in two stages (Figure 4). Stage 1 is characterized by high-frequency, low-displacement forethrusting and high-displacement backthrusting (Figures 4 and 5). Stage 2 is marked by low-frequency, high-displacement forethrusting and low-displacement backthrusting. These stages are comparable with those proposed by Storti et al. (2000) and Bigi et al. (2010), who describe a first stage marked by a sequence of small-scale thrusts that nucleated at the subduction slot, and a second stage with a growing initial wedge that reaches a critical height and behaves as a backstop for further frontal accretion, leading to the trenchward migration of the deformation front.

3.1 Geometry

Geometrical parameters of the wedge, including height (H_{w0} and H_{w1}), width (L_w), and surface slope angle(α_0, α_1, and α_2) (Figure 3), were measured from digital images for representative runs of experiments A1–A4 (Figure 6). The uplift rate of the wedge height (H_{w0}) generally decreased after the transition from stage 1 to 2 (Figure 6a). Exp. A1 without sedimentation showed a slightly lower uplift rate (0.25 cm/cm) than Exp. A2–A4 with sedimentation (0.32–0.45 cm/cm). However,

the rates during stage 2 are nearly the same (0.07–0.09 cm/cm) in all experiments (Exp. A1–A4).

The wedge width (L_w) increases with shortening in a step-like pattern, and increases abruptly when a new forethrust nucleates, but gradually decreases until another forethrust emerges (Figure 6b). This pattern closely correlates with the slope angle (α) of the wedge, which also reflects the cyclicity of forethrust development (Figure 6c). The changes in slope angle indicate a non-steady-state evolution, which contrasts with the critical taper theory of self-similar growth that suggests shape should be conserved. However, the range of slope angles is close to the critical taper angle estimated from the material properties used in this study (e.g., Dahlen, 1984). If a dry and cohesionless wedge follows the critical taper model, the critical taper angle α can be calculated from

$$\alpha = \psi_b - \psi_0 \tag{1}$$

with

$$\psi_0 = \frac{1}{2}\arcsin\frac{\sin\alpha}{\sin\phi} - \frac{1}{2}\alpha \tag{2}$$

$$\psi_b = \frac{1}{2}\arcsin\frac{\sin\phi_b}{\sin\phi} - \frac{1}{2}\phi_b \tag{3}$$

$$\phi = \arctan(\mu) \tag{4}$$

$$\phi_b = \arctan(\mu_b) \tag{5}$$

where μ is the coefficient of internal friction of the wedge with a range from 0.589 to 0.675, and μ_b is the basal friction coefficient (0.47). Therefore, the critical zone of the taper angle ranges between 8.7° and 10.6°. The average slope angle α_0 of Exp. A1-2 during stage 2 falls within this critical zone, and the lower limit is nearly at the minimum critical taper angle (Figure 6c). Exp. A2–A4 also show a similar cyclicity for the slope angle α_0, but the angles are sometimes lower than the minimum critical angle (<8.7°).

When the wedges are divided into inner and outer parts (Figure 3), the slope angle of the outer wedge (α_1) correlates with the cyclicity in wedge shape. The slope

angle (α_1) reaches a minimum when new forethrusts are initiated, as predicted by critical taper theory (Figure 6d). In contrast, the slope angle of the inner wedge (α_2) gradually decreases as shortening increases (Figure 6d). The angles α_2 for experiments with sedimentation (Exp. A2–A4) ultimately become negative.

3.2 Forethrusts and backthrusts

The shortening length required for the transition from stage 1 to 2 shows a positive correlation with the amount of sedimentation. The transition from stage 1 to 2 for Exp. A1 ($n = 2$) occurred after 8.9 ± 0.1 cm shortening, which is the greatest shortening among the experiments of this study (Figure 7). For other experiments with sedimentation, the shortening lengths required to initiate the transition from stage 1 to 2 were 7.7 ± 0.9 cm for Exp. A2 ($n = 7$), 7.2 ± 0.9 cm for Exp. A3 ($n = 4$), and 8.2 ± 0.6 cm for Exp. A4 ($n = 3$). The smallest amount of shortening, as observed in Exp. A3, corresponds to the largest amount of sediment input during stage 1 (Figure 7). However, Exp. A4 received the smallest amount of sediment during stage 1 but showed the greatest shortening among Exp. A2–A4.

The shortening length required for the nucleation of a new forethrust is similar for all experiments in stage 1 (Figure 8). The shortest mean length is 1.6 ± 0.5 cm for Exp. A1 and 1.7 ± 0.5 cm for Exp. A2 . Exp. A3 (2.1 ± 0.5 cm) and A4 (2.0 ± 0.3 cm) yielded slightly greater lengths than those for Exp. A1 and A2, but the intervals for all of the cases overlap with the standard deviation of the mean. Distinct differences in forethrust intervals can be recognized between Exp. A1 and other experiments in stage 2. The interval for Exp. A1 (5.2 ± 0.5 cm) is about 40% smaller than those for Exp. A2 (7.2 ± 1.2 cm), A3 (7.1 ± 1.6 cm), and A4 (7.7 ± 1.4 cm). Shortening lengths are quite varied for each run, and no systematic difference can be found with respect to the variation in sediment input.

A backthrust (BT_i) is a major structural boundary between undeformed sediment layers in the retro-wedge basin and the compressively deformed inner wedge (e.g., Silver & Reed, 1988; Byrne et al., 1993). In this study, there is a large difference in the displacement rate of the backthrusts in the inner wedge (BT_i)between Exp. A1 and the other experiments (Figure 5). The rate for Exp. A1 during stage 2 is 0.10 cm/cm, while those for Exp. A2–A4 are 0.03–0.04 cm/cm. In

stage 1, all of the experiments show a similar trend with an average displacement rate of 0.22 cm/cm.

3.3 Stratigraphy and Wedge Deformation

In this subsection, we analyze one run from each case of Exp. A1–A4 to describe the details of wedge deformation (Figures 9–12) and basin stratigraphy (Figure 13).

3.3.1 Exp. A1-2: No Sediment Supply

In Exp. A1-2, wedge growth was achieved by cycles of alternating wedge lengthening and thickening (Figures 6), which included the following steps: (1) strain was concentrated in the incoming layer at the wedge front prior to the initiation of a new forethrust (Figure 9a), (2) a flat ramp fold at the wedge front formed when a forethrust nucleated at a dipping angle of 25° with a conjugate backthrust at a dipping angle of 40° (Figure 9b, d, and f), (3) an increase in wedge length reduced the surface slope angle (Figure 9b, d, and f), (4) the root of the forethrust was dragged landward by underthrusting and the hanging wall was accreted to the wedge front (Figure 9c and e), (5) underthrusting thickened the wedge with occasional reactivation of pre-existing forethrusts to restore the taper angle (e.g., T_5 in Figure 9c), and (6) gradual narrowing of the wedge resulted in a steeper surface slope.

The final structure of the wedge was characterized by a sequence of forethrusts with uniform spacing (Figure 9). The minimum values of slope angles α_0 and α_1 were close to the minimum critical taper angle at 8.7° (Figure 6d). The backthrust of the inner wedge (BT_i) was active throughout the experiments (Figure 5).

3.3.2 Exp. A2-4: Constant Sediment Supply

In Exp. A2-4, the forethrusts of stage 2 propagated trenchward in a similar manner to those in Exp. A1. A flat ramp fold popped up, and this inverted triangle zone was dragged landward and accreted to the wedge front while being underthrusted (Figure 10). Each thrust sheet was thicker than in Exp. A1 due to syntectonic sedimentation on the hanging wall and wedge front (Figure 10c and d).

Since sediment filled the retro-wedge basin, the backthrusts BT_i were situated more trenchward than those in Exp. A1-2 (Figure 10b). Each forethrust (T_5, T_6, or T_7) was accompanied by a backthrust that developed in the hanging wall during frontal accretion and underthrusting (Figure 10b–d).

For every 2 cm of shortening, a constant amount of sand was delivered to the topographic lows of the retro-wedge basin, the wedge-top basin, and the wedge front (Figure 2). During stage 1 (Figure 13a), most of the input sand was used to fill the retro-wedge basin. After the transition to stage 2 (10–14 cm of shortening), the sand was deposited on the wedge-top basin corresponding to the initiation of forethrust T_5. This wedge-top basin filled up quickly and the rest of the sand overflowed to the wedge front (14 cm of shortening). New accommodation space in the trench-slope (piggy-back) basin emerged by activation of T_6, and the depositional site prograded trenchward (18 cm of shortening). A similar overfill of the trench-slope basin was recognized at 22 cm and 26 cm of shortening. Overall, the depocenter migrated trenchward as the progressive progradation of the deformation extended trenchward. Sediment that filled the retro-wedge basin was mostly undeformed, while sedimentary layers in the trench-slope basins were compressed due to small-scale backthrusting (Figure 10).

3.3.3 Exp. A3-4: Fluctuating Sediment Supply

In Exp. A3-4, a large input of sand during the early stage of the experiment (Figure 2) meant that the transition from deformation stage 1 to 2 occurred earlier than in the other experiments (Figure 7). Three forethrusts (T_4–T_6) were generated during stage 2, and T_5 had a relatively long phase of activity (8.3 cm of shortening) compared with the average of all of the forethrusts in stage 2 (7.0 cm) (Figure 8). Underthrusting of T_5 created a roof thrust in the incoming layer that was covered with sand that had overflowed from the wedge-top basin. This underthrusting caused a reactivation and landward rotation of T_4 and uplift P_b, resulting in a combined wedge-top and retro-wedge basin (Figure 11c and d). The thrust tip of T_5 propagated trenchward as a splay fault and a trishear zone formed in response to the input of sand at the wedge front, resulting in a decrease in the forethrust dip from 21 to 14° (Figure 14). During the displacement on T_6, shortening and thickening caused reactivation of T_5 and the related backthrust BT_o (Figure 11f). Finally,

underthrusting of the incoming layer and the thrust sheet between T_5 and T_6 raised and tilted the outer wedge landward, creating more accommodation space on the wedge top as a forearc basin (Figure 11f).

Sedimentation prior to 10 cm of shortening, which corresponds to the first peak in sediment supply (Figure 2), filled the retro-wedge basin and draped the thrust sheet of T_4 (Figure 13b). Displacement on T_4 led to uplift of the cover sediments, which created a topographic barrier that trapped sediments as a wedge-top basin (10–14 cm of shortening in Figure 13b). Some of the sediment supplied during the second peak (14–20 cm of shortening) bypassed the wedge-top basin and thickened the incoming layer that was in turn emplaced within the thrust sheets between T_5 and T_6 (18–22 cm of shortening in Figure 13b). As continuous uplift of the outer-arc high (a break point in the surface slope of the wedge, P_b in Figure 11) created a large increase in accommodation space on the inner wedge, the final stage of sedimentation filled this combined wedge-top/retro-wedge basin (26 cm of shortening in Figures 13b).

3.3.4 Exp. A4-5: Inversely Fluctuating Sediment Supply

In Exp. A4-5, only two forethrusts (T_4 and T_5) were generated during stage 2, which reflects the large time interval between fault formation events (Figure 8). Fault splays were formed at the thrust tip of T_4 in response to sediment input at the wedge front (Figure 12b–d). The dip angle of forethrust T_4 gradually decreased from 25° when the forethrust developed fault splays to 12.7° at 14 cm of shortening. Underthrusting of T_5 progressively rotated the thrust sheet of T_4 landward and uplifted the outer wedge P_b to the same height as P_a, generating a combined wedge-top/retro-wedge basin and yielding a slope break (Figure 12f). Finally, the wedge behaved as a single body with a forethrust (T_5) and a backthrust (BT_i).

Since there was a low rate of sediment input at the beginning of the experiments (2–6 cm of shortening), the retro-wedge basin was underfilled during stage 1 (Figures 13c). The large amount of sediment delivered during the first peak of sediment input filled both the wedge-top basin and the retro-wedge basin (10–14 cm of shortening). The sediment that overflowed to the wedge front (trench) thickened the incoming layer, and the fault tip developed splays during this period

(Figure 12b–d). Activity on forethrusts T_4 and T_5, accompanied by a long stage of underthrusting, resulted in the formation of a wide area of accommodation space on top of the wedge. However, during the second stage of maximum sediment input, the lack of accommodation space on the wedge top resulted in thickening of the trench-fill sediments (22–26 cm of shortening).

4 Discussion

4.1 Mechanical Analysis

Syntectonic surface processes (sedimentation and erosion) can influence the state of stress of the deforming wedge, such as the differential stress between the maximum and minimum principal stresses and the shear stress acting on the basal décollement (e.g., Simpson, 2010; Fillon, Huismans, van der Beek, & Muñoz, 2013). In this study, we calculated these stresses from the wedge surface slope (α_0 and α_1) and wedge height (H_{w_0} and H_{w_1}), based on the assumption that the wedge follows the critical taper theory (Dahlen, 1984, 1990) (Figure 15). The differential stress $\frac{1}{2}(\sigma_1 - \sigma_3)$ and basal shear stress τ_b were calculated using the following equations:

$$\frac{1}{2}(\sigma_1 - \sigma_3) = \frac{\rho g H_w \cos\alpha \sec 2\psi_0}{\csc\phi \sec 2\psi_0 - 1} \tag{6}$$

$$\tau_b = -\mu_\mathrm{g}\sigma_n \tag{7}$$

with

$$\sigma_1 = \sigma_z - \frac{1}{2}(\sigma_z - \sigma_x)(1 + \sec 2\psi_0) \tag{8}$$

$$\sigma_3 = \sigma_z - \frac{1}{2}(\sigma_z - \sigma_x)(1 - \sec 2\psi_0) \tag{9}$$

$$\sigma_n = \sigma_z - \tau_{xz}\sin 2\alpha - \frac{1}{2}(\sigma_z - \sigma_x)(1 - \cos 2\alpha) \tag{10}$$

$$\sigma_z = -\rho g H_w \cos\alpha \tag{11}$$

$$\tau_{xz} = \frac{1}{2}(\sigma_z - \sigma_x)\tan 2\psi_0 \tag{12}$$

$$\frac{1}{2}(\sigma_z - \sigma_x) = \frac{-\sigma_z}{\csc\phi \cdot \sec 2\psi_0 - 1} \tag{13}$$

where σ_1 and σ_3 are the maximum and minimum principal stresses, respectively; ψ_0 is derived from eq. (2); μ_g is the friction coefficient of the basal décollement; σ_n

399 is the normal stress; and τ_{xz} is the shear stress along the x axis. These equations
400 indicate that both of the differential stress and the basal shear stress are functions
401 of α and H_w, meaning that the absolute value of the differential stress increases as
402 the wedge height H_w increases or the slope angle α decreases. In contrast, the basal
403 shear stress increases if H_w and/or α increase.

404 The differential stress in each experiment showed a progressive increase
405 with shortening (Figure 16a). For example, Exp. A2-4 shows a step-wise increase
406 in differential stress both at P_a and P_b after 8 cm of shortening (Figure 16b),
407 which seems to correlate with sediment input. Similarly, Exp. A3-4 shows that
408 differential stress at P_a stays constant for a certain period (21–25 cm of shortening
409 in Figure 16c), which corresponds to the stage without significant sedimentation
410 (Figure 6a).

411 The basal shear stress shows a similar temporal trend to the differential stress.
412 In Exp. A1-2, which was dominated by frontal accretion throughout the experiment,
413 the basal shear stress shows a gradual increase with shortening, but the shear stress
414 acting at the base of the inner wedge (P_a) is always greater than that at the outer
415 wedge (P_b) (Figure 16a). In contrast, as was demonstrated in Exp. A3 and A4 with
416 prolonged stages of underthrusting , the basal shear stress at the outer wedge (P_b)
417 exceeds that at the inner wedge (P_a) for the period before the second forethrust T_5
418 had initiated (12 cm in Exp. A3 in Figure 16c and 16 cm in Exp. A4 in Figure 16d).

419 Figures 6 and 16 indicate that syntectonic sedimentation contributed to
420 increases in wedge height (H_{w1}) and the slope angle (α_1) of the outer wedge.
421 These responses might have led to spatial variations in the basal shear stress
422 along the décollement and influenced the dominant mode of deformation, such
423 as underthrusting or frontal accretion. A similar result has been reported by
424 Del Castello et al. (2004), who suggested that variations in the basal shear
425 resistance due to an increase in normal stress perturbed the deformation path of
426 the wedge. Temporal variations in coupling along the plate interface may change the
427 deformation pattern of the wedge, which could influence the basin stratigraphy.

428 The basal stress temporally drops with the nucleation cycles of new forethrusts
429 (Figure 16). This characteristic is comparable with the drop in normal stress or

external work force when a new thrust is initiated, as predicted by numerical simulations (Del Castello & Cooke, 2007; McBeck et al., 2017, 2018).

4.2 Sedimentation and Deformation

4.2.1 Retro-wedge Basin

The smaller shortening length required for the transition from stage 1 to stage 2 with syntectonic sedimentation (Exp. A2–A4) could be ascribed to additional loading in the retro-wedge basin (Figure 7). The addition of the downward gravitational force and frictional force parallel to the backstop surface strengthens the shear stress at the base of the inner wedge and enhances the mechanical stability of the rear of the initial wedge (Figure 17). The rapid decrease in the displacement rate of the backthrust (BT_i) after the transition to stage 2 (Exp. A2–A4 in Figure 5) could also be related to this additional gravitational force (cf. Silver & Reed, 1988). Thus, sedimentation in the retro-wedge basin might relate to segmentation of the wedge, characterized by an outer wedge in a critical state of stress and an inner wedge in a stable state (Lohrmann et al., 2003) that acts as a dynamic backstop (cf. Kopp & Kukowski, 2003). This may generate backthrusting in the outer wedge (BT_o) instead of having BT_i accommodate a component of the landward deformation of the wedge. The landward deformation associated with BT_o for Exp. A2–A4 could account for the lower angle of the wedge-top slope α_2 (Figures 10–12). In addition, the downward force acting on the backstop increases the possibility of having the backstop subside or rotate, which would lead to a step-down of the décollement, underplating of the subducting sediments, or tectonic erosion (Strasser et al., 2009; Kimura et al., 2011; Mannu et al., 2017).

A shorter length of shortening required for the transition from stage 1 to stage 2 in the case of syntectonic sedimentation (Exp. A2–A4) could be ascribed to additional loading in the retro-wedge basin (Figure 7). Addition of the gravitational force downward and the frictional force parallel to the backstop surface strengthens the shear stress at the base of the inner wedge and enhances the mechanical stability of the rear side of the initial wedge (Figure 17). Rapid decrease of the displacement rate of the backthrust (BT_i) after the transition to stage 2 (Exp. A2–A4 in Figure 5) could also be related with this additional gravitational force (cf. Silver & Reed,

1988). This effect would be correlated to the wedge segmentation composed of outer wedge in a critical state of stress and inner wedge in a stable state (Lohrmann et al., 2003), as a dynamic backstop (cf. Kopp & Kukowski, 2003). This may stimulate development of backthrusting in the outer wedge (BT_o) instead of using the BT_i to accommodate a component of the landward deformation of the wedge. Landward deformation associated with BT_o for Exp. A2–A4 could be a reason for a lower angle of the wedge top slope α_2 (Figures 10–12). In addition, downward force acting on the backstop increases a possibility to subside or rotate the backstop, and then to lead the décollement step-down, underplating of the subducting sediments, or tectonic erosion (Strasser et al., 2009; Kimura et al., 2011; Mannu et al., 2017).

4.2.2 Wedge-top Basin

An increase in the normal and basal shear stress beneath the outer wedge due to underthrusting of the incoming layer plus surface sedimentation would lead to a frictional contrast between the inner and outer wedges (Figures 17 and 18). Strong coupling of the interface between the outer wedge and the décollement could dominate the underthrusting phase, with movement on the pre-existing forethrust causing uplift of the outer wedge. Once the outer-arc high (P_b) is uplifted to a point higher than the axial zone (P_a), the wedge-top basin is combined with the retro-wedge basin to generate a wide accommodation space on top of the wedge.

Previous studies have suggested that a significant amount of sediment loading could make the wedge supercritical and therefore devoid of internal deformation (Davis et al., 1983; Liu et al., 1992; Storti & McClay, 1995; Stockmal et al., 2007; Simpson, 2010; Fillon, Huismans, & van der Beek, 2013). However, our experiments showed that the sediment layers in the wedge-top basin deformed internally in response to rotation of the main forethrust and small-scale backthrusts in the hanging wall (Figures 11f and 12d). In the present study, the sediment load on the wedge-top basin was not sufficient to make the wedge supercritical.

4.2.3 Wedge Front (Trench)

The thickness of the incoming layer on the subducting plate shows a positive correlation with forethrust spacing (Liu et al., 1992; Marshak & Wilkerson, 1992;

Contardo et al., 2011). The wide spacing and reduced number of forethrusts in Exp. A2–A4, in contrast to Exp. A1 (Figures 9–12 and 17), could be partly due to the amount of sediment on the incoming layer at the wedge front. Underthrusting of the thickened incoming layer could amplify rotation of the pre-existing thrust sheet and uplift the outer-arc high (Figure 18c). This response could increase the likelihood of the wedge-top basin combining with the trench-slope basin(s) to form a large forearc basin.

Another result of the present study is that sedimentation at the wedge front could temporarily seal the toe of the frontal thrust, which may result in a splay fault propagating from the fault tip (Figure 14). The formation of splay faults at the thrust tip owing to a gradual decrease in the thrust angle could be related to a trishear-style propagation of the fault tip towards the surface (footwall triangular shear zone), most likely in response to the sedimentation volume (Erslev, 1991; Hardy & Allmendinger, 2011). Although the splay faults extended along the length of the slip plane, stable sliding on the active fault plane may still be favorable for the nucleation of a new forethrust at a trenchward site (Del Castello & Cooke, 2007). The mechanical weakness of uncompacted sand supplied at the wedge front may be another factor that influenced the behavior of fault tips at the wedge front.

4.3 Balance between Sedimentary Supply and Accommodation Space

The amount and location of sediment deposition on the deforming wedge depend on the balance between the quantity of sediment delivered from the hinterland and the amount of accommodation space on the wedge. The sediment is typically deposited from turbidity currents and submarine landslides, which are closely correlated with eustacy, climate, and tectonics, as these fators ultimately control sediment production and transportation. For example, eustatic sea level fluctuations, especially during regression stages, can cause large amounts of sediment to be transported directly into submarine canyons (e.g., Blum & Hattier-Womack, 2009). On tectonic time scales, mountain building or magmatic flare-ups along convergent plate boundaries can result in the production of large amounts of sediment (e.g., Larsen et al., 2014; Ducea et al., 2015, 2017). In this study, we attempted to simulate deposition of sediment sourced from the hinterland across

the strike of the subduction zone, and therefore did not consider the direct input of sediment to the trench from a different source. However, trench-fill sediment at the wedge front is commonly supplied from lateral (transverse) and axial (longitudinal) flows in natural forearcs. The transverse sediment supply is characterized by turbidity currents in submarine canyons that incise into a deforming accretionary wedge with the development of submarine fans in and around the trench. The Cascadia subduction zone is an example of this tectonic setting where large amounts of sediment fill the trench-slope basins and overflow sediment widely covers the trench, forming submarine fans (e.g., Goldfinger et al., 2017). Submarine landslides at the frontal wedge slope provide another source of sediment to the wedge front (Yamada et al., 2010), and are typically observed at sediment-starved, erosive margins such as the Middle America Trench (von Huene et al., 2000; Harders et al., 2011), the northern Hikurangi margin (Collot et al., 2001) and the Japan Trench (Strasser et al., 2013). In contrast, the longitudinal sediment supply is controlled by trench-parallel turbidity currents sourced from drainage areas with high sediment production, as reported at Sumatra (Moore et al., 1982), eastern Makran (Bourget et al., 2011), Nankai (Pickering et al., 1992), the southern Hikurangi margin (Lewis et al., 1998), and the southern Lesser Antilles (Limonta et al., 2015). For the case of the Nankai Trough, subduction of thickened trench-fill sediment may cause out-of-sequence thrusting and uplift of the outer-arc high (Moore et al., 2015; Mannu et al., 2017).

The accommodation space on the wedge is controlled by the pattern of wedge growth, including alternating frontal accretion and underthrusting. When frontal accretion is dominant (Exp. A1 and A2), a series of small trench-slope basins develops trenchward (Figures 17 and 18b). In contrast, the dominance of the underthrusting phase (Exp. A3 and A4) causes uplift of the outer wedge and results in the formation of a large accommodation space on the wedge top (Figures 17 and 18c). Therefore, the forearc basin stratigraphy could be controlled by the relative balance between sediment supply and the creation of accommodation space on the wedge. Even if a large accommodation space is created by uplift of the outer-arc high, minor sediment input to the forearc results in an underfilled basin such as Lombok basin along the Sunda arc (Lüschen et al., 2011). On the other hand, a large sediment supply from the hinterland, as reported for the Cascadia forearc

(Beeson et al., 2017), would fill the accommodation space on the wedge and result in a great thickness of trench-fill sediment, leading to a wide spacing between thrusts and between trench-slope basins.

4.4 Interactions between Surface Processes and Wedge Deformation

The greater shear stress at the base of the outer wedge compared with the inner wedge ($\tau_{b_0} < \tau_{b_1}$) could strengthen coupling of the interface between the wedge base and the décollement layer, leading to slip along the pre-existing forethrust surface rather than the nucleation of a new forethrust (Figure 17). The inversion of basal shear resistance could prolong underthrusting of the incoming layer and limit frontal accretion. Numerical simulations have indicated that high basal friction could extend the duration of the underthrusting phase (Burbidge & Braun, 2002; McBeck et al., 2017). Such underthrusting has been observed at Nankai (Moore et al., 2014), northern Barbados (Moore et al., 1995), and Alaska (Li et al., 2018), where undeformed trench-fill sediments on an underthrusting slab are located behind a subducting structural high. Prolonged underthrusting drags the incoming layer landward and causes the surface slope α_1 to increase. The stratigraphy in the wedge-top basin tilts landward and the depocenter migrates landward (Figure 18c).

When basal shear stress is lower at the outer wedge than the inner wedge ($\tau_{b_0} > \tau_{b_1}$), the initiation of a new forethrust at the wedge front means that deformation propagates trenchward (Figure 17). This scenario can lead to a low amount of uplift of the outer-arc high, a positive surface slope of α_2, and a lack of accommodation space on top of the wedge. In this case, most of the sediment supplied from the hinterland is redirected trenchward, resulting in trenchward migration of the depocenter (Figures 17 and 18b).

Although underthrusting results in an increase in the slope angle at the wedge front α_1, when the angle reaches a critical value the mode of wedge growth switches to frontal accretion in order to decrease the taper angle (Figure 17). This change results in a cessation of uplift of the outer-arc high and stabilizes the pre-existing wedge. Most of the sediment sourced from the hinterland bypasses the wedge-top basin if it is overfilled and becomes trapped in a newly developed trench-slope basin.

Previous studies have invoked external factors to explain the prolonged underthrusting and creation of slope breaks in accretionary wedges, including the subduction of high frictional materials (Mulugeta & Koyi, 1992; Lohrmann et al., 2003; Miyakawa et al., 2010), variations in the cohesion of the wedge (Zhao et al., 1986), subduction of a topographic high such as a seamount (Lallemand et al., 1992; Morgan & Bangs, 2017), and bending of the subducting oceanic plate (Fuller et al., 2006). However, the present results suggest that syntectonic sedimentation can lead to a heterogeneous distribution of stress at the décollement; i.e., a higher basal shear stress on the trenchward side of the wedge relative to the landward side. This implies that the slope break on the wedge surface could be generated even in the case of a uniform décollement without any change in subduction (e.g., velocity) of the roughness or material properties of the subducting slab.

5 Conclusions

We performed a series of sandbox analogue experiments to examine how the pattern of stratigraphy in a forearc basin responds to deformation of an accretionary wedge with syntectonic sedimentation and how the pattern of wedge deformation is influenced by sedimentation on the wedge surface. Basin stratigraphy was found to be controlled by the dominance of frontal accretion or underthrusting during the deformation phase. When frontal accretion was dominant, the wedge deformation prograded trenchward along with the depocenter. In contrast, when the underthrusting phase was prolonged, the incoming layer of the footwall uplifted the outer wedge and an outer-arc high emerged. This caused the sediment layers deposited on the wedge top to tilt landward and the depocenter to migrate landward. Syntectonic sedimentation had a number of effects on wedge deformation, including (1) faster stabilization of the inner wedge by filling of the retro-wedge basin and (2) longer intervals between forethrust nucleation. Syntectonic sedimentation on the wedge surface could cause variations in the basal shear stress along the décollement, changing the style of wedge deformation (i.e., frontal accretion vs. underthrusting) and basin evolution (i.e., trenchward vs. landward migration of the depocenter). The results show that basin stratigraphy depends on the growth pattern of the accretionary wedge and that sedimentation alone can determine the mode of deformation of the wedge.

Acknowledgments

This study was supported by a Grant-in-Aid for Scientific Research from the Japan Society for the Promotion of Science (JSPS) (17K05687). Relevant multimedia data files for this study are available on Figshare (http://doi.org/10.6084/m9.figshare.10271294).

References

Adam, J., Urai, J., Wieneke, B., Oncken, O., Pfeiffer, K., Kukowski, N., ... Schmatz, J. (2005). Shear localisation and strain distribution during tectonic faulting—new insights from granular-flow experiments and high-resolution optical image correlation techniques. *Journal of Structural Geology*, *27*(2), 283–301. doi: 10.1016/j.jsg.2004.08.008

Albert, F., Kukowski, N., Tassara, A., & Oncken, O. (2018). Material transfer and subduction channel segmentation at erosive continental margins: Insights from scaled analogue experiments. *Tectonophysics*, *749*, 46–61. doi: 10.1016/j.tecto.2018.10.019

Beeson, J. W., Goldfinger, C., & Fortin, W. F. (2017). Large-scale modification of submarine geomorphic features on the Cascadia accretionary wedge caused by catastrophic flooding events. *Geosphere*, *13*(5), 1713–1728. doi: 10.1130/GES01388.1

Bigi, S., Di Paolo, L., Vadacca, L., & Gambardella, G. (2010). Load and unload as interference factors on cyclical behavior and kinematics of Coulomb wedges: Insights from sandbox experiments. *Journal of Structural Geology*, *32*(1), 28–44. doi: 10.1016/j.jsg.2009.06.018

Blum, M. D., & Hattier-Womack, J. (2009). Climate change, sea-level change, and fluvial sediment supply to deepwater depositional systems. In B. Kneller, O. J. Martinsen, & B. McCaffrey (Eds.), *External Controls on Deep-Water Depositional Systems* (Vol. 92, pp. 15–39). Tulsa, Oklahoma, United States: SEPM (Society for Sedimentary Geology). doi: 10.2110/sepmsp.092.015

Bourget, J., Zaragosi, S., Ellouz-Zimmermann, N., Mouchot, N., Garlan, T., Schneider, J.-L., ... Lallemant, S. (2011). Turbidite system architecture and sedimentary processes along topographically complex slopes: the Makran convergent margin. *Sedimentology*, *58*(2), 376–406. doi: 10.1111/j.1365-3091.2010.01168.x

Buiter, S. J. H. (2012). A review of brittle compressional wedge models. *Tectonophysics*, *530–531*, 1–17. doi: 10.1016/j.tecto.2011.12.018

Burbidge, D. R., & Braun, J. (2002). Numerical models of the evolution of accretionary wedges and fold-and-thrust belts using the distinct–element method. *Geophysical Journal International*, *148*(3), 542–561. doi:

10.1046/j.1365-246x.2002.01579.x

Byrne, D. E., Davis, D. M., & Sykes, L. R. (1988). Loci and maximum size of thrust earthquakes and the mechanics of the shallow region of subduction zones. *Tectonics*, *7*(4), 833–857. doi: 10.1029/TC007i004p00833

Byrne, D. E., Wang, W.-h., & Davis, D. M. (1993). Mechanical role of backstops in the growth of forearcs. *Tectonics*, *12*(1), 123–144. doi: 10.1029/92TC00618

Collot, J.-Y., Lewis, K., Lamarche, G., & Lallemand, S. (2001). The giant Ruatoria debris avalanche on the northern Hikurangi margin, New Zealand: Result of oblique seamount subduction. *Journal of Geophysical Research*, *106*, 19271–19297. doi: 10.1029/2001JB900004

Contardo, X. J., Kukowski, N., & Cembrano, J. M. (2011). Material transfer and its influence on the formation of slope basins along the south central chilean convergent margin: Insights from scaled sandbox experiments. *Tectonophysics*, *513*, 20–36. doi: 10.1016/j.tecto.2011.09.016

Cruz, L., Malinski, J., Hernandez, M., Take, A., & Hilley, G. (2011). Erosional control of the kinematics of the Aconcagua fold-and-thrust belt from numerical simulations and physical experiments. *Geology*, *39*(5), 439–442. doi: 10.1130/G31675.1

Dahlen, F. A. (1984). Noncohesive critical coulomb wedges: An exact solution. *Journal of Geophysical Research*, *89*(B12), 10125–10133. doi: 10.1029/JB089iB12p10125

Dahlen, F. A. (1990). Critical taper model of fold-and-thrust belts and accretionary wedges. *Annual Review of Earth and Planetary Sciences*, *18*(1), 55–99. doi: 10.1146/annurev.ea.18.050190.000415

Davis, D., Suppe, J., & Dahlen, F. A. (1983). Mechanics of fold-and-thrust belts and accretionary wedges. *Journal of Geophysical Research*, *88*(B2), 1153–1172. doi: 10.1029/JB088iB02p01153

Del Castello, M., & Cooke, M. L. (2007). Underthrusting-accretion cycle: Work budget as revealed by the boundary element method. *Journal of Geophysical Research*, *112*(B12404). doi: 10.1029/2007JB004997

Del Castello, M., Pini, G. A., & McClay, K. R. (2004). Effect of unbalanced topography and overloading on Coulomb wedge kinematics: Insights from sandbox modeling. *Journal of Geophysical Research*, *109*(B5). doi:

10.1029/2003JB002709

Dotare, T., Yamada, Y., Adam, J., Hori, T., & Sakaguchi, H. (2016). Initiation of a thrust fault revealed by analog experiments. *Tectonophysics*, *684*, 148–156. doi: 10.1016/j.tecto.2015.12.023

Ducea, M. N., Bergantz, G. W., Crowley, J. L., & Otamendi, J. (2017). Ultrafast magmatic buildup and diversification to produce continental crust during subduction. *Geology*, *45*(3), 235–238. doi: 10.1130/G38726.1

Ducea, M. N., Paterson, S. R., & DeCelles, P. G. (2015). High-volume magmatic events in subduction systems. *Elements*, *11*(2), 99–104. doi: 10.2113/gselements.11.2.99

Erslev, E. A. (1991). Trishear fault-propagation folding. *Geology*, *19*(6), 617–620. doi: 10.1130/0091-7613(1991)019$¡$0617:TFPF$¿$2.3.CO;2

Fillon, C., Huismans, R. S., & van der Beek, P. (2013). Syntectonic sedimentation effects on the growth of fold-and-thrust belts. *Geology*, *41*(1), 83–86. doi: 10.1130/G33531.1

Fillon, C., Huismans, R. S., van der Beek, P., & Muñoz, J. A. (2013). Syntectonic sedimentation controls on the evolution of the southern Pyrenean fold-and-thrust belt: Inferences from coupled tectonic-surface processes models. *Journal of Geophysical Research: Solid Earth*, *118*, 5665–5680. doi: 10.1002/jgrb.50368

Fuller, C. W., Willett, S. D., & Brandon, M. T. (2006). Formation of forearc basins and their influence on subduction zone earthquakes. *Geology*, *34*(2), 65–68. doi: 10.1130/G21828.1

Goldfinger, C., Galer, S., Beeson, J., Hamilton, T., Black, B., Romsos, C., ... Morey, A. (2017). The importance of site selection, sediment supply, and hydrodynamics: A case study of submarine paleoseismology on the northern Cascadia margin, Washington USA. *Marine Geology*, *384*, 4–46. doi: 10.1016/j.margeo.2016.06.008

Graveleau, F., & Dominguez, S. (2008). Analogue modelling of the interaction between tectonics, erosion and sedimentation in foreland thrust belts. *Comptes Rendus Geoscience*, *340*(5), 324–333. doi: 10.1016/j.crte.2008.01.005

Graveleau, F., Malavieille, J., & Dominguez, S. (2012). Experimental modelling of orogenic wedges: A review. *Tectonophysics*, *538–540*, 1–66. doi: 10.1016/j

.tecto.2012.01.027

Gutscher, M.-A., Kukowski, N., Malavieille, J., & Lallemand, S. (1996). Cyclical behavior of thrust wedges: Insights from high basal friction sandbox experiments. *Geology*, *24*(2), 135–138. doi: 10.1130/0091-7613(1996)024$¡$0135:CBOTWI$¿$2.3.CO;2

Gutscher, M.-A., Kukowski, N., Malavieille, J., & Lallemand, S. (1998). Material transfer in accretionary wedges from analysis of a systematic series of analog experiments. *Journal of Structural Geology*, *20*(4), 407–416. doi: 10.1016/S0191-8141(97)00096-5

Harders, R., Ranero, C. R., Weinrebe, W., & Behrmann, J. H. (2011). Submarine slope failures along the convergent continental margin of the Middle America Trench. *Geochemistry, Geophysics, Geosystems*, *12*(6), 1–26. doi: 10.1029/2010GC003401

Hardy, S., & Allmendinger, R. W. (2011). Trishear: A review of kinematics, mechanics, and applications. In K. McClay, J. Shaw, & J. Suppe (Eds.), *Thrust Fault-Related Folding* (pp. 95–119). American Association of Petroleum Geologists. doi: 10.1306/1334M943429

Hardy, S., Duncan, C., Masek, J., & Brown, D. (1998). Minimum work, fault activity and the growth of critical wedges in fold and thrust belts. *Basin Research*, *10*(3), 365–373. doi: 10.1046/j.1365-2117.1998.00073.x

Hubbert, M. K. (1937). Theory of scale models as applied to the study of geologic structures. *Geological Society of America Bulletin*, *48*(10), 1459–1519. doi: 10.1130/GSAB-48-1459

Hubbert, M. K., & Rubey, W. W. (1959). role of fluid pressure in mechanics of overthrust faulting: I. Mechanics of fluid-filled porous solids and its application to overthrust faulting. *Geological Society of America Bulletin*, *70*(2), 115–166. doi: 10.1130/0016-7606(1959)70[115:ROFPIM]2.0.CO;2

Kimura, G., Moore, G. F., Strasser, M., Screaton, E., Curewitz, D., Streiff, C., & Tobin, H. (2011). Spatial and temporal evolution of the megasplay fault in the Nankai Trough. *Geochemistry, Geophysics, Geosystems*, *12*(Q0A008). doi: 10.1029/2010GC003335

Klinkmüller, M., Schreurs, G., Rosenau, M., & Kemnitz, H. (2016). Properties of granular analogue model materials: A community wide survey. *Tectonophysics*,

684, 23–38. doi: 10.1016/j.tecto.2016.01.017

Konstantinovskaya, E., & Malavieille, J. (2011). Thrust wedges with décollement levels and syntectonic erosion: A view from analog models. *Tectonophysics*, *502*(3–4), 336–350. doi: 10.1016/j.tecto.2011.01.020

Kopp, H., & Kukowski, N. (2003). Backstop geometry and accretionary mechanics of the Sunda margin. *Tectonics*, *22*(6, 1072). doi: 10.1029/2002TC001420

Kukowski, N., & Oncken, O. (2006). Subduction erosion: The "normal" mode of fore-arc material transfer along the Chilean margin? In O. Oncken et al. (Eds.), *The Andes: Active Subduction Orogeny* (pp. 217–236). Berlin, Germany: Springer. doi: 10.1007/978-3-540-48684-8_10

Lallemand, S. E., Malavieille, J., & Calassou, S. (1992). Effects of oceanic ridge subduction on accretionary wedges; experimental modeling and marine observations. *Tectonics*, *11*(6), 1301–1313. doi: 10.1029/92TC00637

Larroque, C., Calassou, S., Malavieille, J., & Chanier, F. (1995). Experimental modelling of forearc basin development during accretionary wedge growth. *Basin Research*, *7*(3), 255–268. doi: 10.1111/j.1365-2117.1995.tb00109.x

Larsen, I. J., Montgomery, D. R., & Greenberg, H. M. (2014). The contribution of mountains to global denudation. *Geology*, *42*(6), 527–530. doi: 10.1130/G35136.1

LaVision. (2012). Product-manual for davis 8.0 strainmaster. [Computer software manual].

Lewis, K. B., Collot, J.-Y., & Lallemand, S. E. (1998). The dammed hikurangi trough: A channel-fed trench blocked by subducting seamounts and their wake avalanches (new zealand-france geodynz project). *Basin Research*, *10*(4), 441–468. doi: 10.1046/j.1365-2117.1998.00080.x

Li, J., Shillington, D. J., Saffer, D. M., Bécel, A., Nedimović, M. R., Kuehn, H., ... Abers, G. A. (2018). Connections between subducted sediment, pore-fluid pressure, and earthquake behavior along the Alaska megathrust. *Geology*, *46*(4), 299–302. doi: 10.1130/G39557.1

Limonta, M., Garzanti, E., Resentini, A., Andò, S., Boni, M., & Bechstädt, T. (2015). Multicyclic sediment transfer along and across convergent plate boundaries (Barbados, Lesser Antilles). *Basin Research*, *27*(6), 696–713. doi: 10.1111/bre.12095

Liu, H., McClay, K. R., & Powell, D. (1992). Physical models of thrust wedges. In K. R. McClay (Ed.), *Thrust Tectonics* (pp. 71–81). London, United Kingdom: Chapman & Hall.

Lohrmann, J., Kukowski, N., Adam, J., & Oncken, O. (2003). The impact of analogue material properties on the geometry, kinematics, and dynamics of convergent sand wedges. *Journal of Structural Geology*, *25*(10), 1691–1711. doi: 10.1016/S0191-8141(03)00005-1

Lüschen, E., Müller, C., Kopp, H., Engels, M., Lutz, R., Planert, L., ... Djajadihardja, Y. S. (2011). Structure, evolution and tectonic activity of the eastern Sunda forearc, Indonesia, from marine seismic investigations. *Tectonophysics*, *508*, 6–21. doi: 10.1016/j.tecto.2010.06.008

Malavieille, J., Larroque, C., & Calassou, S. (1993). Modélisation expérimentale des rélations tectonique/sedimentation entre bassin avant-arc et prisme d'accretion. *Paris, Académie des Sciences, Comptes Rendus*, *316*(II), 1131–1137.

Mannu, U., Ueda, K., Willett, S. D., Gerya, T. V., & Strasser, M. (2016). Impact of sedimentation on evolution of accretionary wedges: Insights from high-resolution thermomechanical modeling. *Tectonics*, *35*(12), 2828–2846. doi: 10.1002/2016TC004239

Mannu, U., Ueda, K., Willett, S. D., Gerya, T. V., & Strasser, M. (2017). Stratigraphic signatures of forearc basin formation mechanisms. *Geochemistry, Geophysics, Geosystems*, *18*(6), 2388–2410. doi: 10.1002/2017GC006810

Marshak, S., & Wilkerson, M. S. (1992). Effect of overburden thickness on thrust belt geometry and development. *Tectonics*, *11*(3), 560–566. doi: 10.1029/92TC00175

McBeck, J. A., Cooke, M. L., Herbert, J. W., Maillot, B., & Souloumiac, P. (2017). Work optimization predicts accretionary faulting: An integration of physical and numerical experiments. *Journal of Geophysical Research: Solid Earth*, *122*(9), 7485–7505. doi: 10.1002/2017JB013931

McBeck, J. A., Cooke, M. L., Souloumiac, P., Maillot, B., & Mary, B. (2018). The influence of detachment strength on the evolving deformational energy budget of physical accretionary prisms. *Solid Earth*, *9*(6), 1421–1436. doi: 10.5194/se-9-1421-2018

Milliman, J. D., & Syvitski, J. P. M. (1992). Geomorphic/tectonic control of sediment discharge to the ocean: The importance of small mountainous rivers. *Journal of Geology*, *100*(5), 525–544. doi: 10.1086/629606

Miyakawa, A., Yamada, Y., & Matsuoka, T. (2010). Effect of increased shear stress along a plate boundary fault on the formation of an out-of-sequence thrust and a break in surface slope within an accretionary wedge, based on numerical simulations. *Tectonophysics*, *484*, 127–138. doi: 10.1016/j.tecto.2009.08.037

Moore, G. F., Boston, B. B., Strasser, M., Underwood, M. B., & Ratliff, R. A. (2015). Evolution of tectono-sedimentary systems in the Kumano Basin, Nankai Trough forearc. *Marine and Petroleum Geology*, *67*, 604–616. doi: 10.1016/j.marpetgeo.2015.05.032

Moore, G. F., Curray, J. R., & Emmel, F. J. (1982). Sedimentation in the Sunda Trench and forearc region. In J. K. Leggett (Ed.), *Trench-Forearc Geology: Sedimentation and Tectonics on Modern and Ancient Active Plate Margins* (Vol. 10, pp. 245–258). London, United Kingdom: Geological Society.

Moore, G. F., Kanagawa, K., Strasser, M., Dugan, B., Maeda, L., Toczko, S., & the IODP Expedition 338 Scientific Party. (2014). IODP Expedition 338: NanTroSEIZE Stage 3: NanTroSEIZE plate boundary deep riser 2. *Scientific Drilling*, *17*, 1–12. doi: 10.5194/sd-17-1-2014

Moore, G. F., Zhao, Z., Shipley, T. H., Bangs, N., & Moore, J. C. (1995). Structural setting of the Leg 156 area, northern Barbados Ridge accretionary prism. In T. H. Shipley, Y. Ogawa, P. Blum, & et al. (Eds.), *Proceedings of the Ocean Drilling Program, Initial Reports* (Vol. 156, pp. 13–27). College Station, TX: Ocean Drilling Program. doi: 10.2973/odp.proc.ir.156.102.1995

Morgan, J. K., & Bangs, N. L. (2017). Recognizing seamount-forearc collisions at accretionary margins: Insights from discrete numerical simulations. *Geology*, *45*(7), 635–638. doi: 10.1130/G38923.1

Mugnier, J. L., Baby, P., Colletta, B., Vinour, P., Bale, P., & Leturmy, P. (1997). Thrust geometry controlled by erosion and sedimentation: A view from analogue models. *Geology*, *25*(5), 427–430. doi: 10.1130/0091-7613(1997)025$¡$0427:TGCBEA$¿$2.3.CO;2

Mulugeta, G., & Koyi, H. (1992). Episodic accretion and strain partitioning in a model sand wedge. *Tectonophysics*, *202*(2), 319–333. doi: 10.1016/0040

-1951(92)90117-O

Noda, A. (2016). Forearc basins: Types, geometries, and relationships to subduction zone dynamics. *Geological Society of America Bulletin*, *128*(5–6), 879–895. doi: 10.1130/B31345.1

Noda, A. (2018). Forearc basin stratigraphy and interactions with accretionary wedge growth according to the critical taper concept. *Tectonics*, *37*(3), 965–988. doi: 10.1002/2017TC004744

Noda, A., Koge, H., Yamada, Y., Miyakawa, A., & Ashi, J. (2019). *Supporting information for "Subduction of trench-fill sediments beneath an accretionary wedges: Insights from sandbox analogue experiments".* doi: 10.6084/m9.figshare.10263674

Perrin, C., Clemenzi, L., Malavieille, J., Molli, G., Taboada, A., & Dominguez, S. (2013). Impact of erosion and décollements on large-scale faulting and folding in orogenic wedges: analogue models and case studies. *Journal of the Geological Society, London*, *170*(6), 893–904. doi: 10.1144/jgs2013-012

Pickering, K. T., Underwood, M. B., & Taira, A. (1992). Open-ocean to trench turbidity-current flow in the Nankai Trough: Flow collapse and reflection. *Geology*, *20*(12), 1099–1102. doi: 10.1130/0091-7613(1992)020$¡$1099:OOTTTC$¿$2.3.CO;2

Santimano, T., Rosenau, M., & Oncken, O. (2015). Intrinsic versus extrinsic variability of analogue sand-box experiments –Insights from statistical analysis of repeated accretionary sand wedge experiments. *Journal of Structural Geology*, *75*, 80–100. doi: 10.1016/j.jsg.2015.03.008

Schellart, W. P., & Strak, V. (2016). A review of analogue modelling of geodynamic processes: Approaches, scaling, materials and quantification, with an application to subduction experiments. *Journal of Geodynamics*, *100*, 7–32. doi: 10.1016/j.jog.2016.03.009

Schumann, K., Behrmann, J. H., Stipp, M., Yamamoto, Y., Kitamura, Y., & Lempp, C. (2014). Geotechnical behavior of mudstones from the Shimanto and Boso accretionary complexes, and implications for the Nankai accretionary prism. *Earth, Planets and Space*, *66*(1), 129. doi: 10.1186/1880-5981-66-129

Silver, E. A., & Reed, D. L. (1988). Backthrusting in accretionary wedges. *Journal of Geophysical Research*, *93*(B4), 3116–3126. doi: 10.1029/JB093iB04p03116

Simpson, G. D. H. (2010). Formation of accretionary prisms influenced by sediment subduction and supplied by sediments from adjacent continents. *Geology*, *38*(2), 131–134. doi: 10.1130/G30461.1

Stockmal, G. S., Beaumont, C., Nguyen, M., & Lee, B. (2007). Mechanics of thin-skinned fold-and-thrust belts: Insights from numerical models. In J. W. Sears, T. A. Harms, & C. A. Evenchick (Eds.), *Whence the Mountains? Inquiries into the Evolution of Orogenic Systems* (Vol. 433, pp. 63–98). Boulder, Colorado, USA: Geological Society of America. doi: 10.1130/2007.2433(04)

Storti, F., & McClay, K. (1995). Influence of syntectonic sedimentation on thrust wedges in analogue models. *Geology*, *23*(11), 999–1002. doi: 10.1130/0091-7613(1995)023$¡$0999:IOSSOT$¿$2.3.CO;2

Storti, F., Salvini, F., & McClay, K. (1997). Fault-related folding in sandbox analogue models of thrust wedges. *Journal of Structural Geology*, *19*(3), 583–602. doi: 10.1016/S0191-8141(97)83029-5

Storti, F., Salvini, F., & McClay, K. (2000). Synchronous and velocity-partitioned thrusting and thrust polarity reversal in experimentally produced, doubly-vergent thrust wedges: Implications for natural orogens. *Tectonics*, *19*, 378–396. doi: 10.1029/1998TC001079

Strasser, M., Kölling, M., Ferreira, C. d. S., Fink, H. G., Fujiwara, T., Henkel, S., ... scientists, J. C. M.-E. (2013). A slump in the trench: Tracking the impact of the 2011 Tohoku-Oki earthquake. *Geology*, *41*(8), 935–938. doi: 10.1130/G34477.1

Strasser, M., Moore, G. F., Kimura, G., Kitamura, Y., Kopf, A. J., Lallemant, S., ... Zhao, X. (2009). Origin and evolution of a splay fault in the Nankai accretionary wedge. *Nature Geoscience*, *2*(9), 648–652. doi: 10.1038/NGEO609

Tsuji, T., Ashi, J., Strasser, M., & Kimura, G. (2015). Identification of the static backstop and its influence on the evolution of the accretionary prism in the Nankai Trough. *Earth and Planetary Science Letters*, *431*, 15–25. doi: 10.1016/j.epsl.2015.09.011

von Huene, R., Ranero, C. R., Weinrebe, W., & Hinz, K. (2000). Quaternary convergent margin tectonics of Costa Rica, segmentation of the Cocos

Plate, and Central American volcanism. *Tectonics*, *19*(2), 314–334. doi: 10.1029/1999TC001143

Wang, W.-H., & Davis, D. M. (1996). Sandbox model simulation of forearc evolution and noncritical wedges. *Journal of Geophysical Research*, *101*(B5), 11329–11339. doi: 10.1029/96JB00101

Wu, J., & McClay, K. (2011). Two-dimensional analog modeling of fold and thrust belts: Dynamic interactions with syncontractional sedimentation and erosion. In K. McClay, J. Shaw, & J. Suppe (Eds.), *Thrust Fault-Related Folding* (pp. 301–333). American Association of Petroleum Geologists. doi: 10.1306/13251343M9450

Yamada, Y., Baba, K., Miyakawa, A., & Matsuoka, T. (2014). Granular experiments of thrust wedges: Insights relevant to methane hydrate exploration at the Nankai accretionary prism. *Marine and Petroleum Geology*, *51*, 34–48. doi: 10.1016/j.marpetgeo.2013.11.008

Yamada, Y., Kaneda, K., & Matsuoka, T. (2006). Influences of material properties on analogue model experiments of geologic structures. *Journal of the Society of Materials Science, Japan*, *55*(5), 452–457. (in Japanese with English abstract) doi: 10.2472/jsms.55.452

Yamada, Y., Yamashita, Y., & Yamamoto, Y. (2010). Submarine landslides at subduction margins: Insights from physical models. *Tectonophysics*, *484*(1), 156–167. doi: 10.1016/j.tecto.2009.09.007

Zhang, Y., Yang, S., Chen, H., Dilek, Y., Cheng, X., Lin, X., ... Zhu, T. (2019). The effect of overburden thickness on deformation mechanisms in the Keping fold-thrust belt, southwestern Chinese Tian Shan Mountains: Insights from analogue modeling. *Tectonophysics*, *753*, 79–92. doi: 10.1016/j.tecto.2019.01.005

Zhao, W. L., Davis, D. M., Dahlen, F. A., & Suppe, J. (1986). Origin of convex accretionary wedges: Evidence from barbados. *Journal of Geophysical Research*, *91*(B10), 10246–10258. doi: 10.1029/JB091iB10p10246

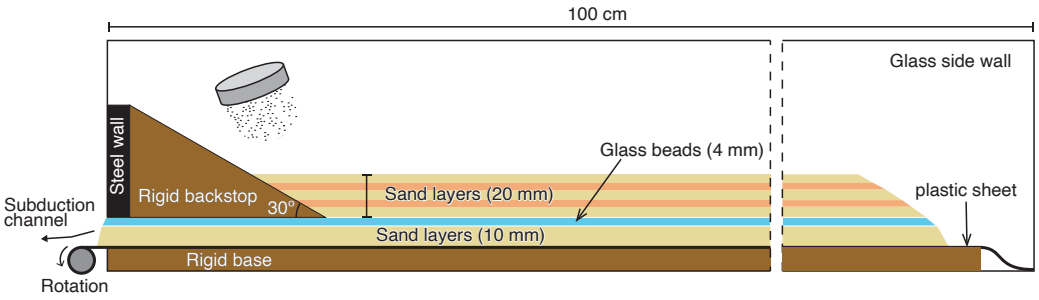

Figure 1. Experimental apparatus of this study.

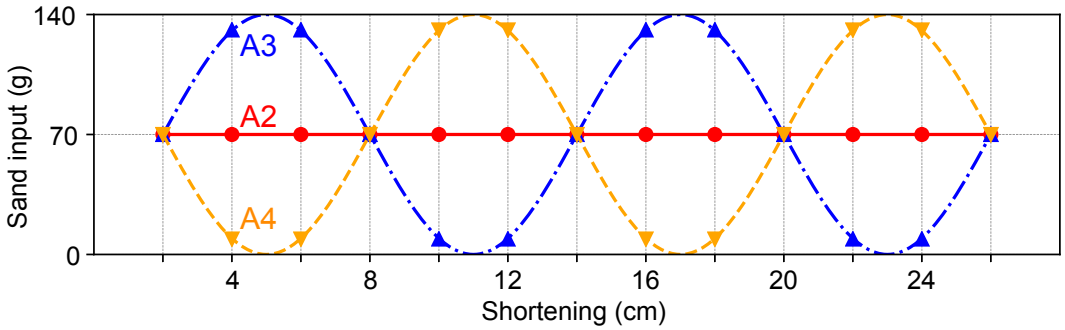

Figure 2. Amounts of sediment input during the experiments. Exp. A2, constant; Exp. A3, fluctuating; Exp. A4, inversely fluctuating.

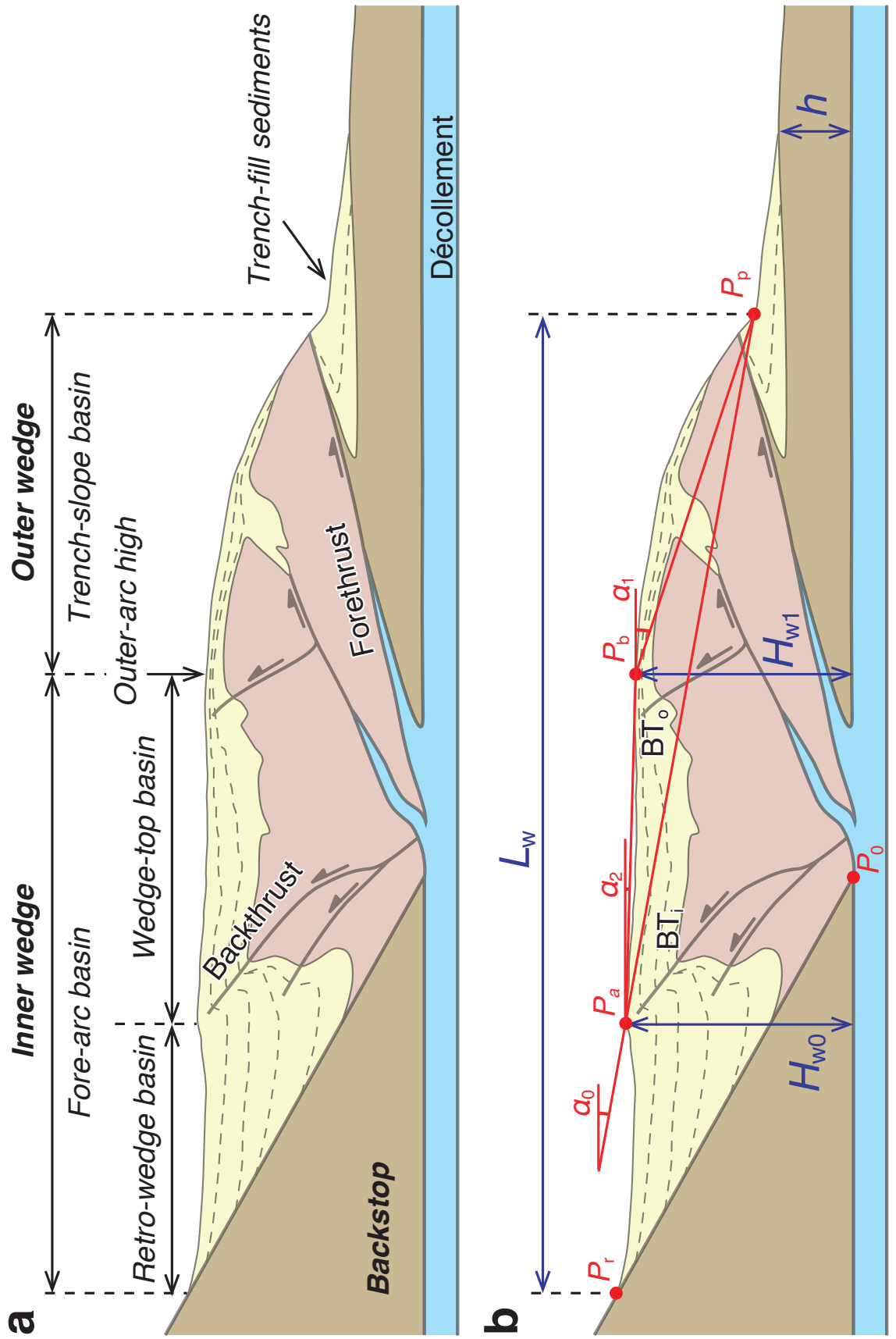

Figure 3. (a) Definition of the terminology used in this study. (b) Geometrical parameters and symbols for reference. L_w, width of the wedge; H_w, height of the wedge; h, thickness of the incoming layer (trench-fill sediment deposited on the subducting plate); P_a, axial point in the inner wedge; P_b, outer-arc high. BT_i and BT_o are backthrusts in the inner wedge and outer wedge, respectively. Slope angles of α_0, α_2, α_2 are the angles between P_p–P_a, P_p–P_b, and P_a–P_b, respectively.

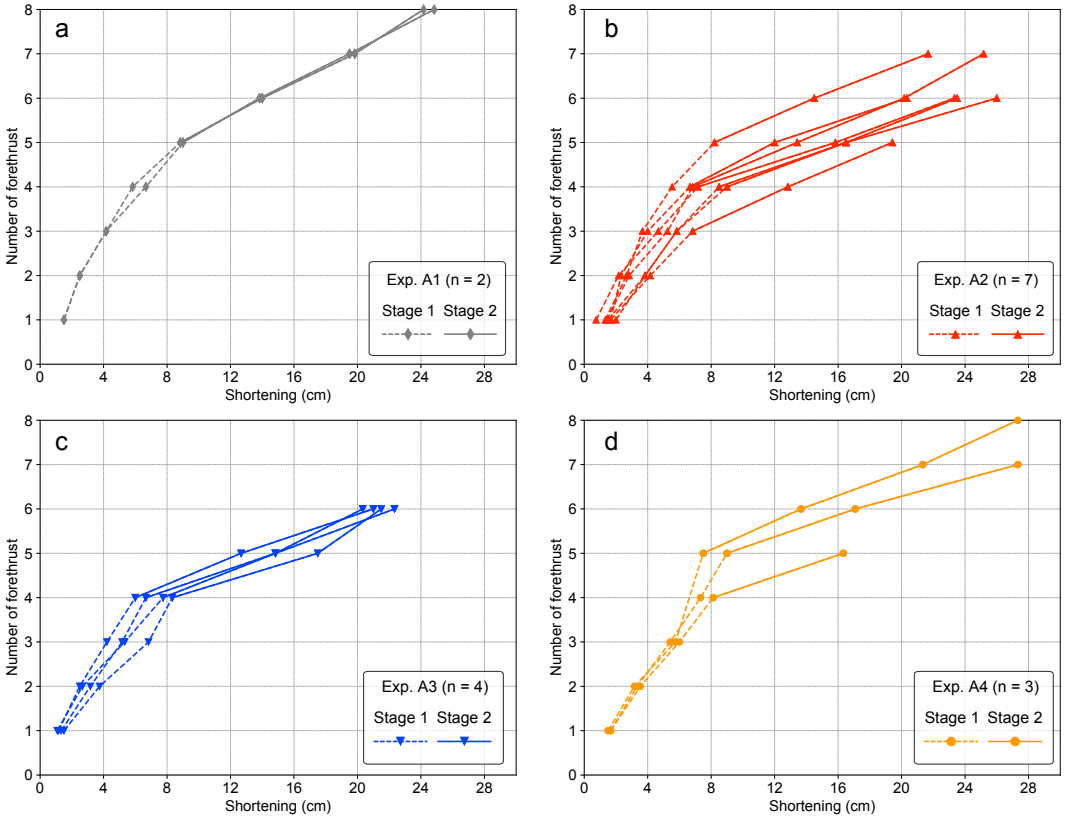

Figure 4. Number of forethrusts with shortening (cm) for all experiments. (a) Experiment without sedimentation (Exp. A1). (b) Experiment with constant sedimentation (Exp. A2). (c) Experiment with fluctuating sedimentation (Exp. A3). (d) Experiment with inversely fluctuating sedimentation (Exp. A4).

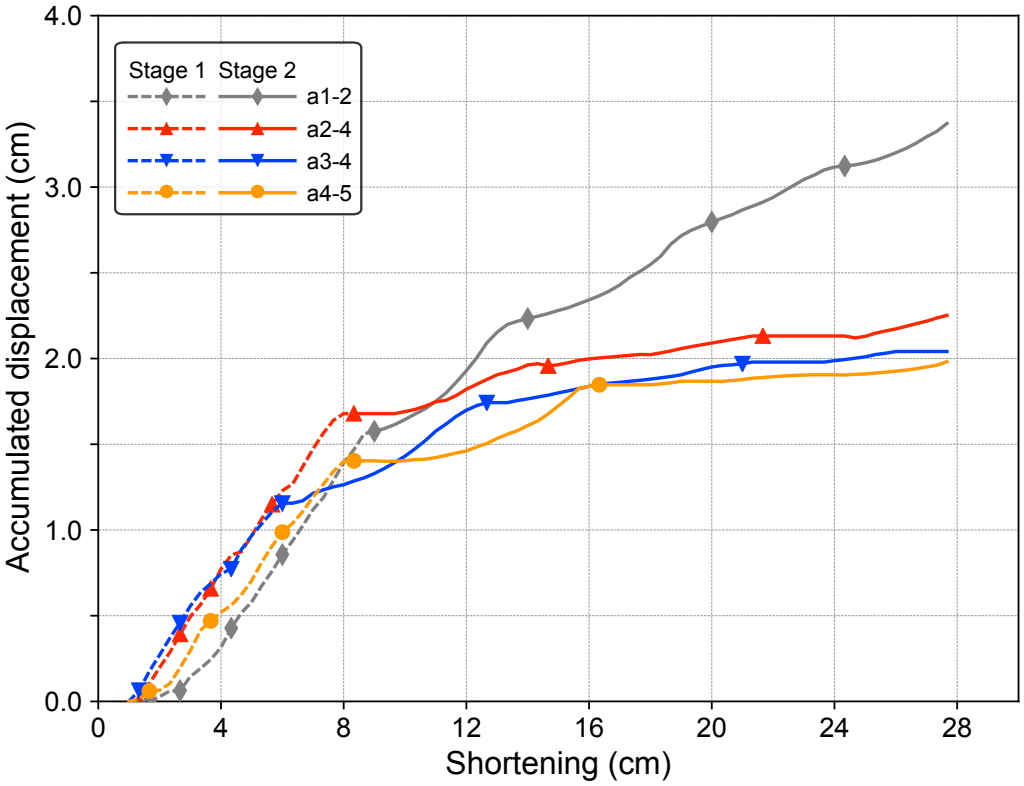

Figure 5. Accumulated displacement on a backthrust of the inner wedge (BT_i).

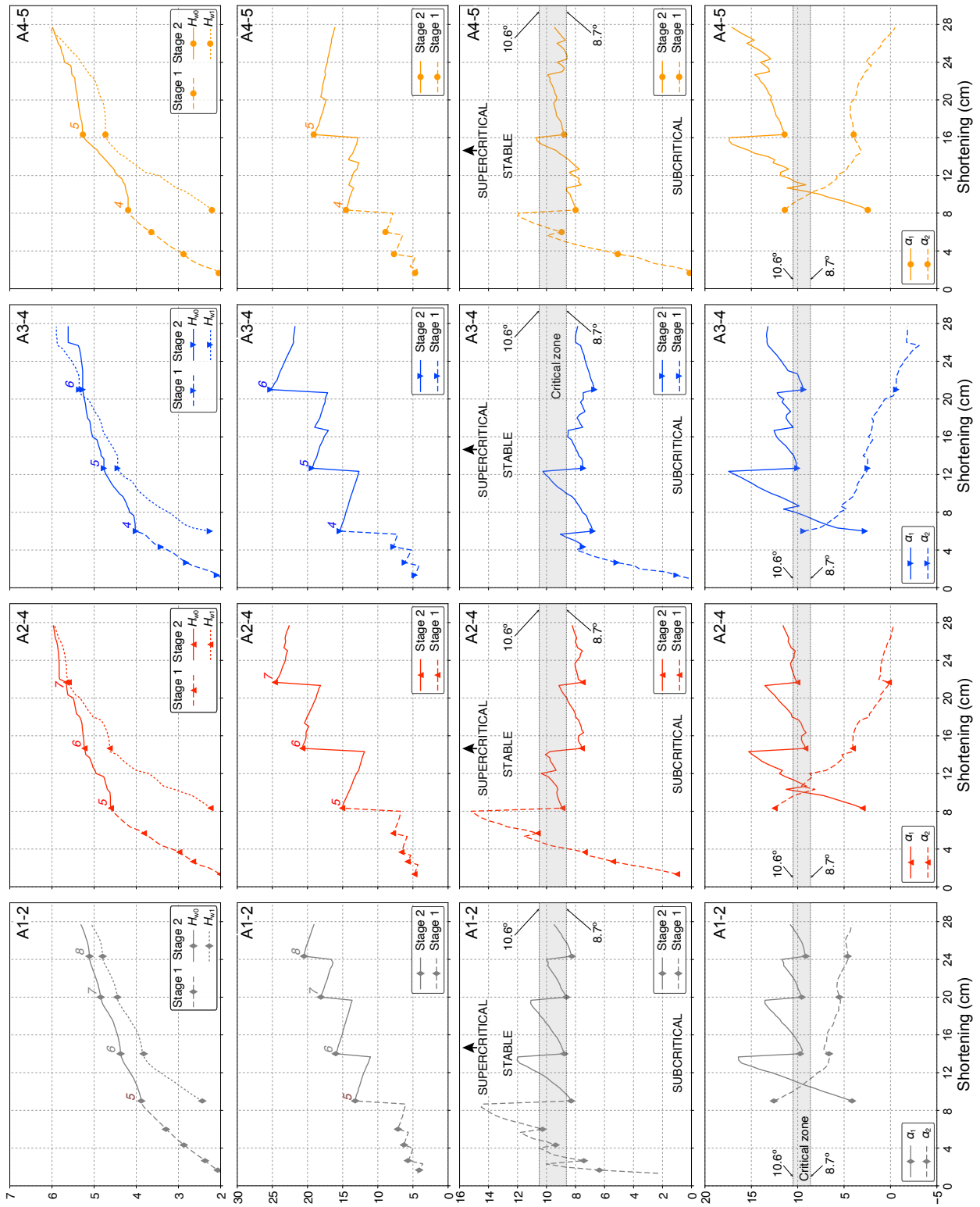

Figure 6. Geometrical parameters of wedges for representative runs. (a) Wedge height, H_{w0} and H_{w1}. (b) Wedge width, L_w. (c) Average taper angle of the entire wedge, α_0. (d) Slope angles of the outer wedge (α_1) and the inner wedge (α_2). Symbols with numbers indicate the nucleation points of forethrusts. Grayish bands in (c) and (d) indicate critical zones of the taper angle calculated based on critical taper theory (cf. Dahlen, 1984).

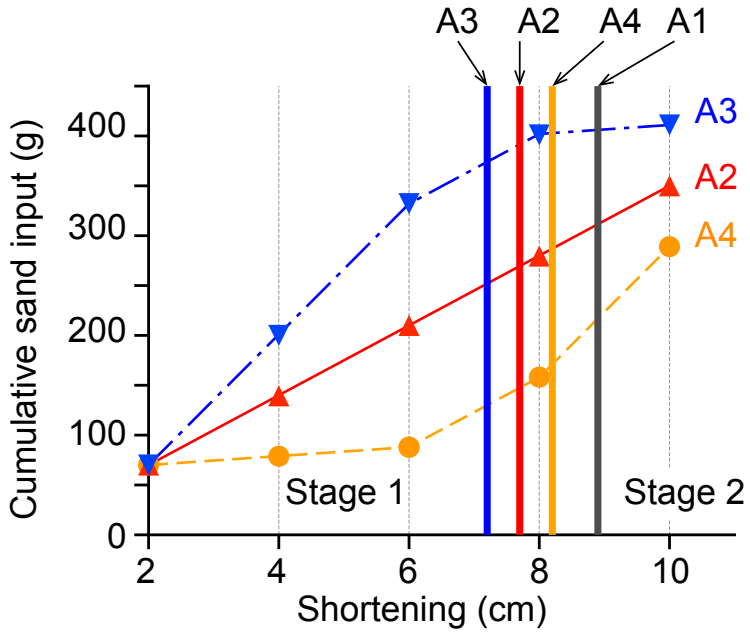

Figure 7. Shortening lengths required to initiate the transition from stage 1 to 2 (horizontal axis). Amounts of cumulative sediment input for Exp. A2–A4 (vertical axis).

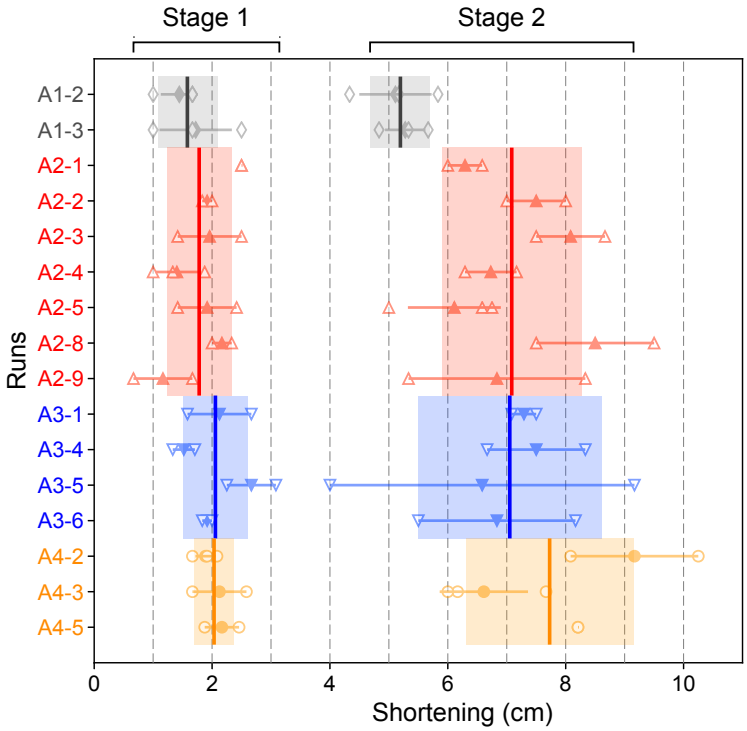

Figure 8. Intervals of forethrust nucleation in stages 1 and 2 for all runs. Open and solid symbols indicate individual and mean intervals for each run, respectively. Solid vertical lines and shaded area indicate the averages and standard deviations of the mean, respectively, of the shortening lengths for forethrust intervals for each case from Exp. A1 to Exp. A4.

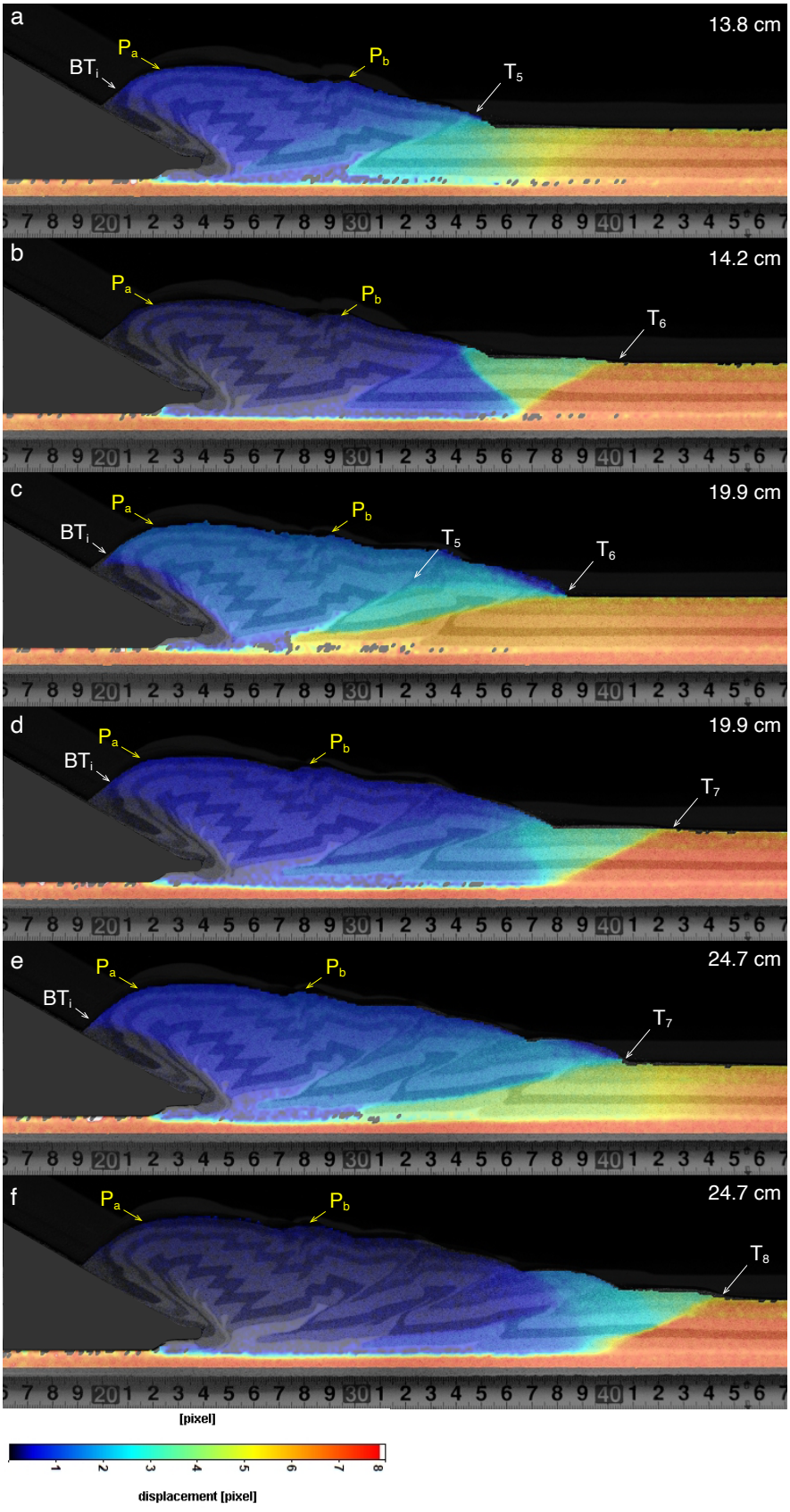

Figure 9. Representative images of incremental displacement (velocity length) obtained from DIC analysis for Exp. A1-2.

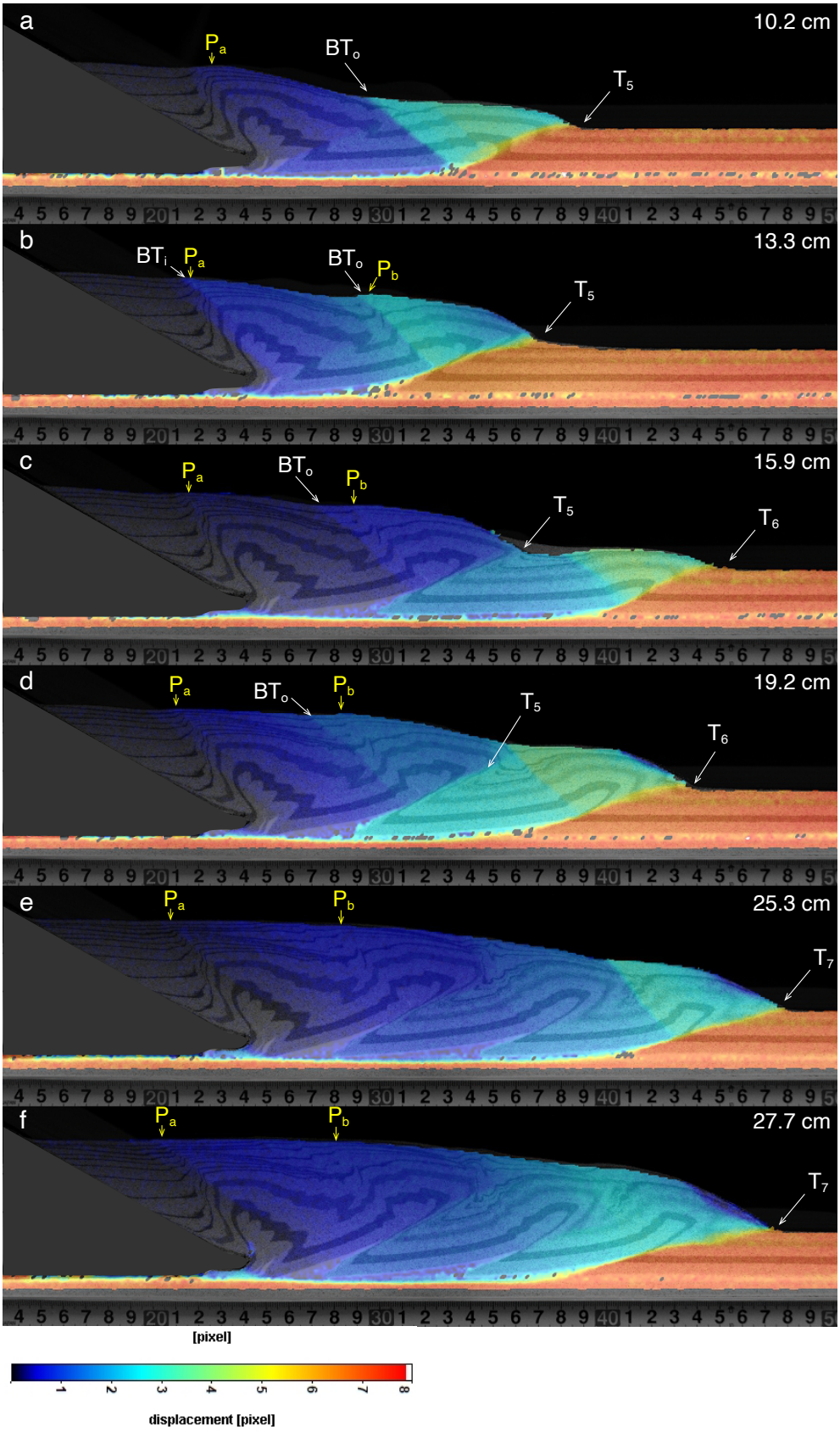

Figure 10. Representative images of incremental displacement (velocity length) obtained from DIC analysis for Exp. A2-4.

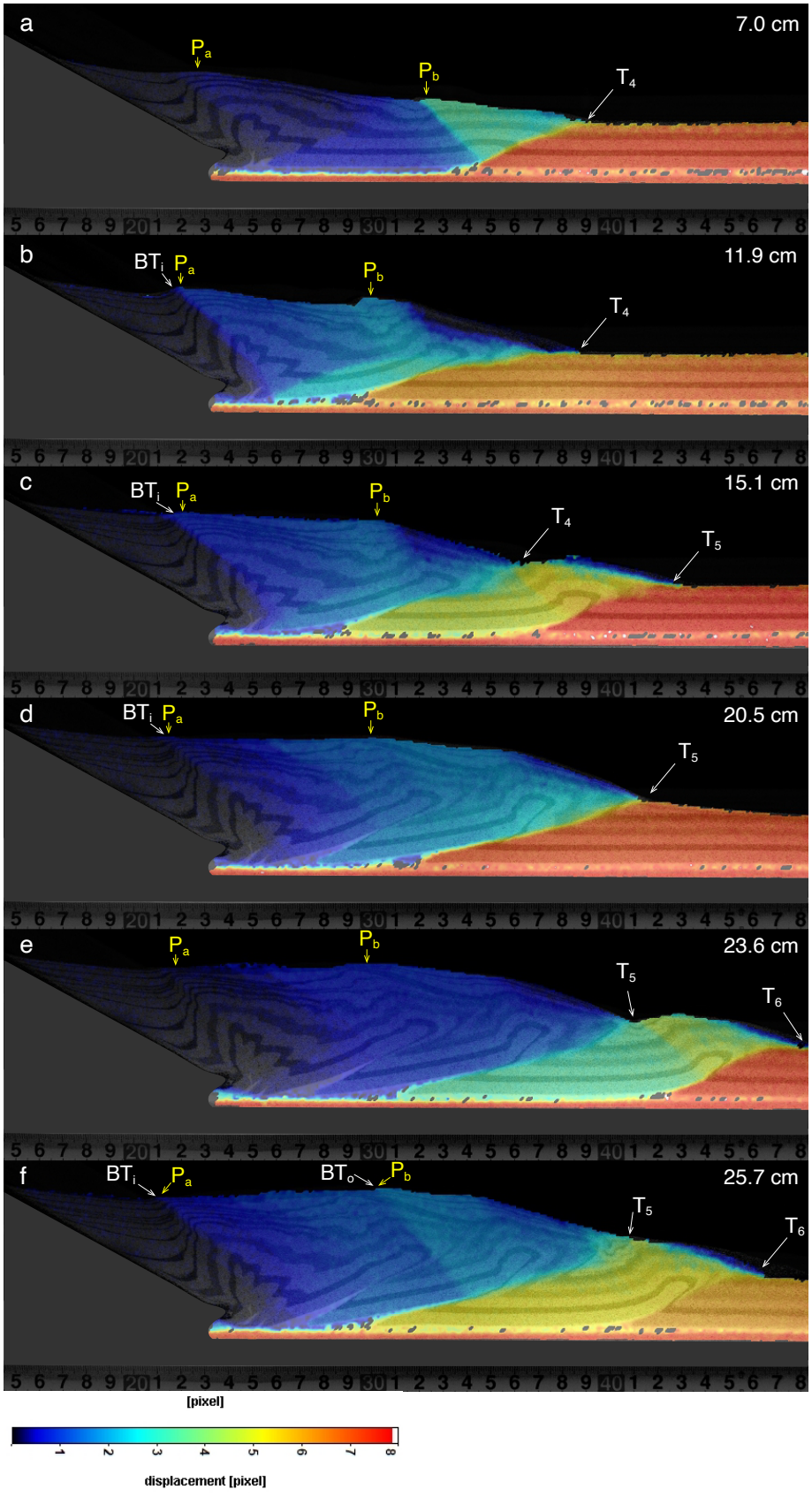

Figure 11. Representative images of incremental displacement (velocity length) obtained from DIC analysis for Exp. A3-4.

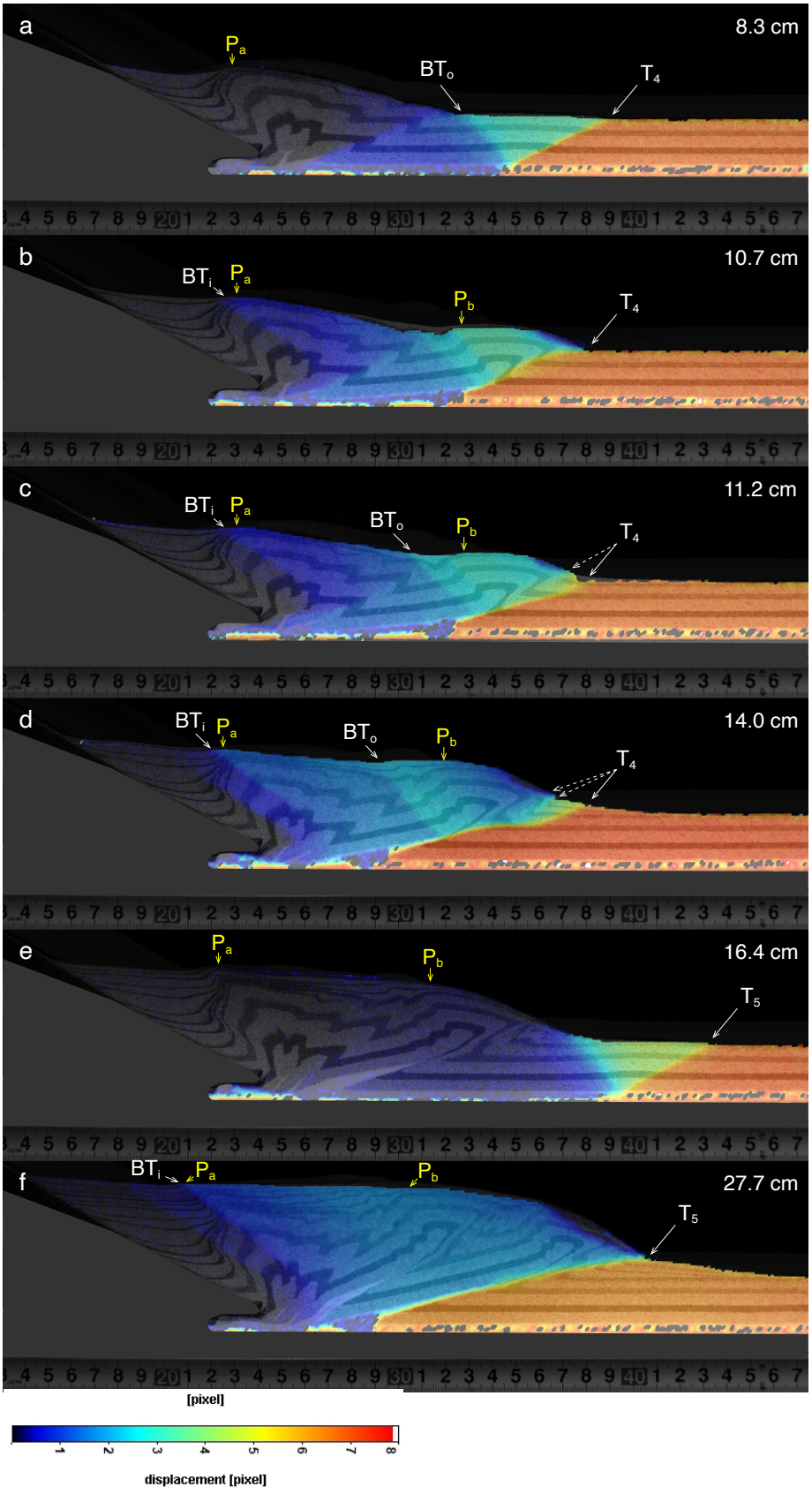

Figure 12. Representative images of incremental displacement (velocity length) obtained from DIC analysis for Exp. A4-5.

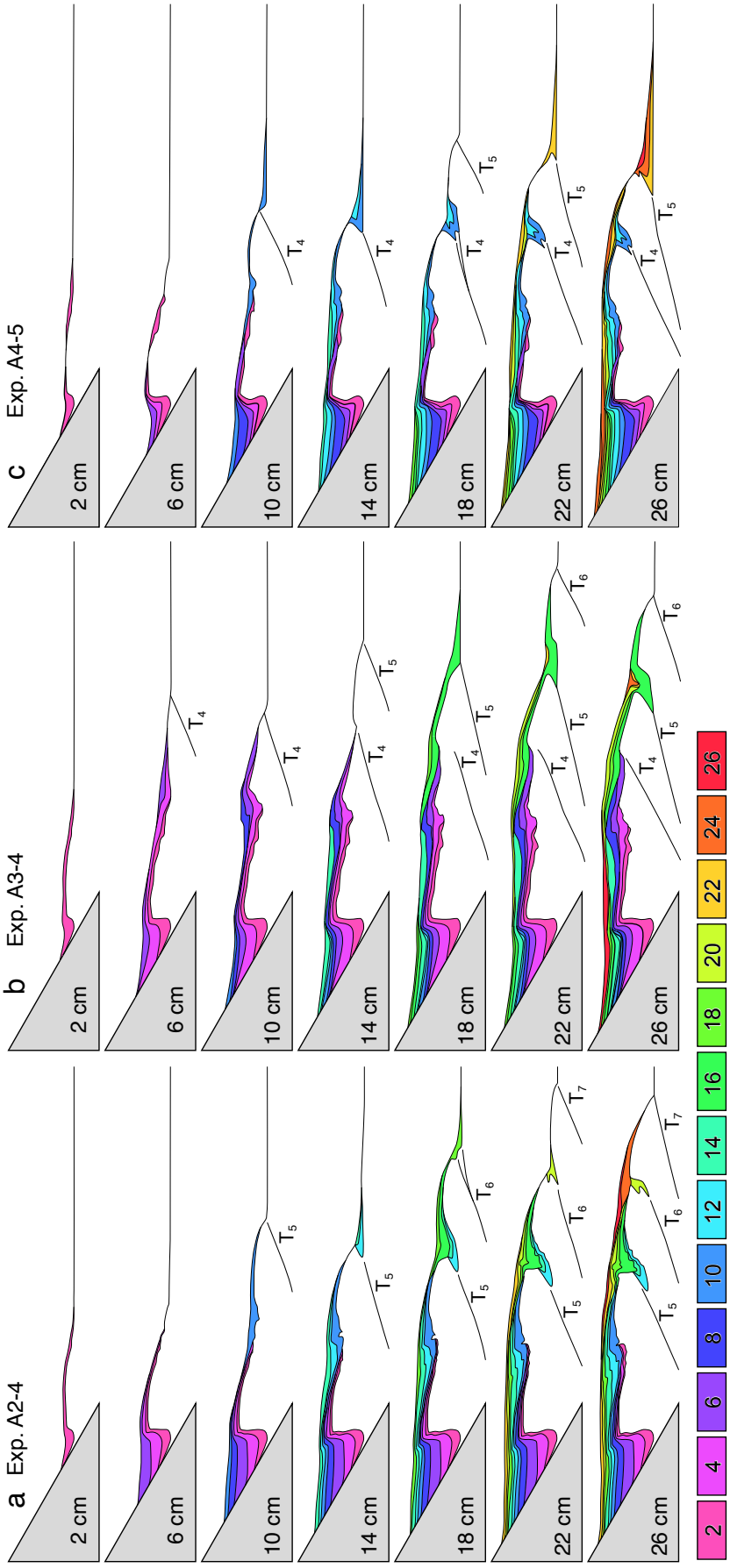

Figure 13. Traces of basin stratigraphy for every 4 cm of shortening.

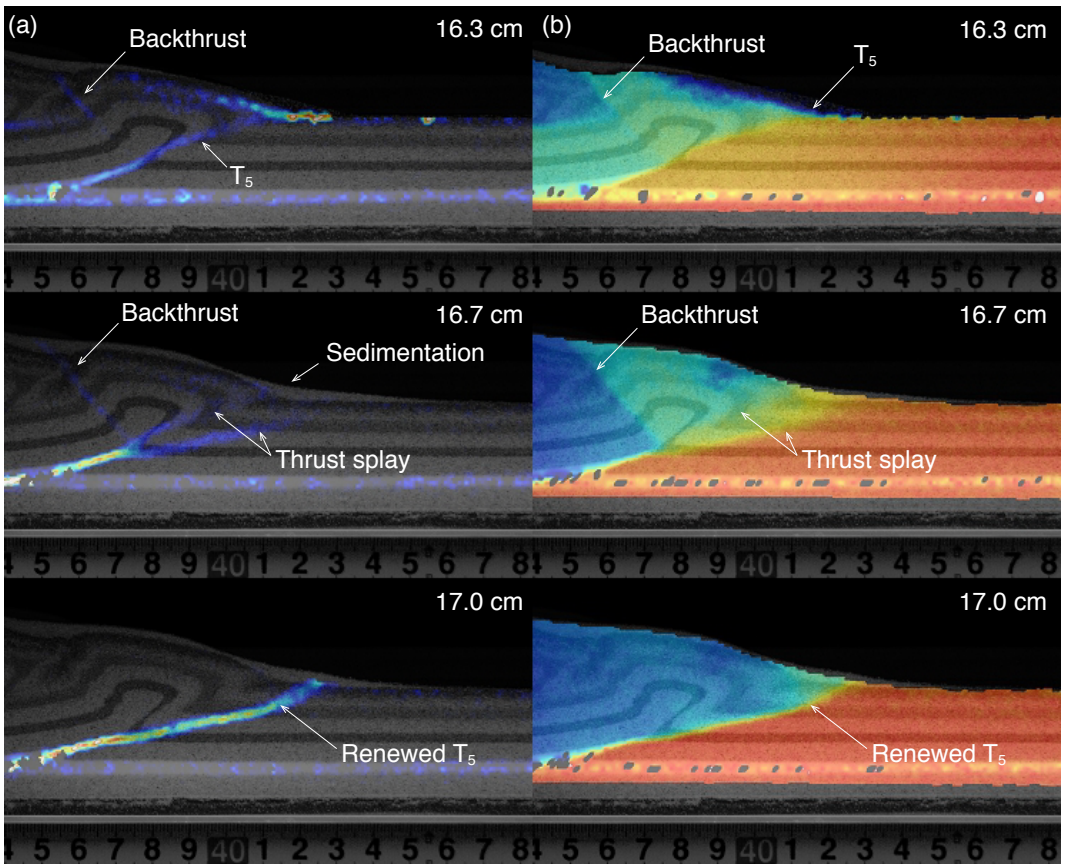

Figure 14. Time-series DIC images showing splay faults from the forethrust tip (Exp. A3-4). (a) Shear strength. (b) Incremental displacement (velocity length).

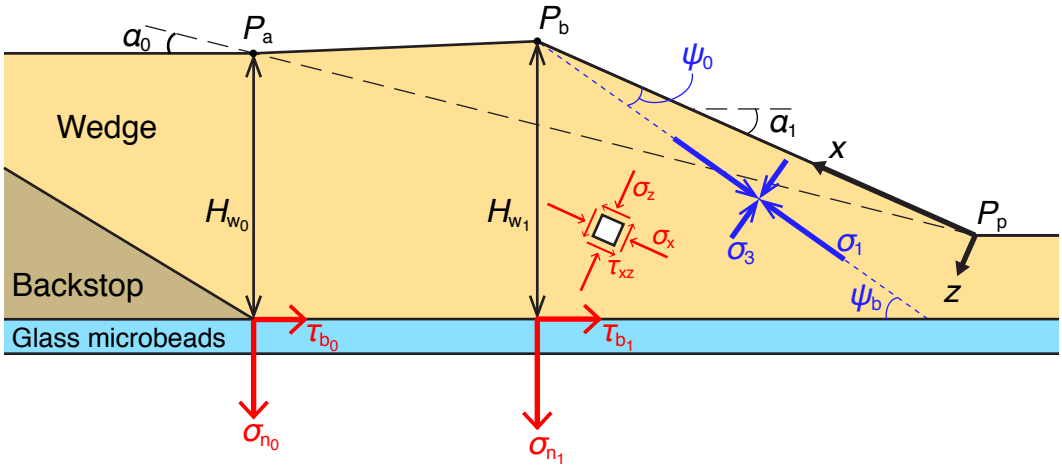

Figure 15. Cross-section of an accretionary wedge with coordinate axes x and z, and angles α_0, α_1, ψ_0, and ψ_b. The angle between the maximum principal stress σ_1 and the coordinate axis x is ψ_0.

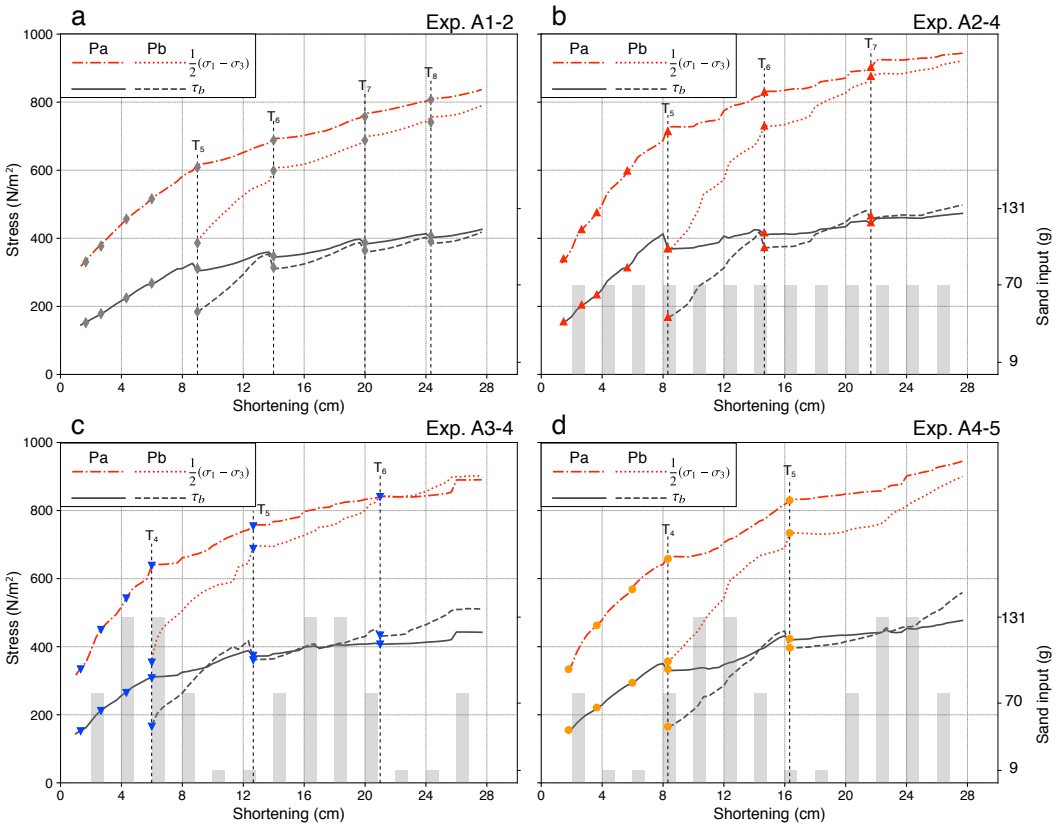

Figure 16. Differential stress $1/2(\sigma_1 - \sigma_3)$ and shear stress τ_b at the bases of P_a and P_b (left vertical axis) and amount of sediment input (right vertical axis).

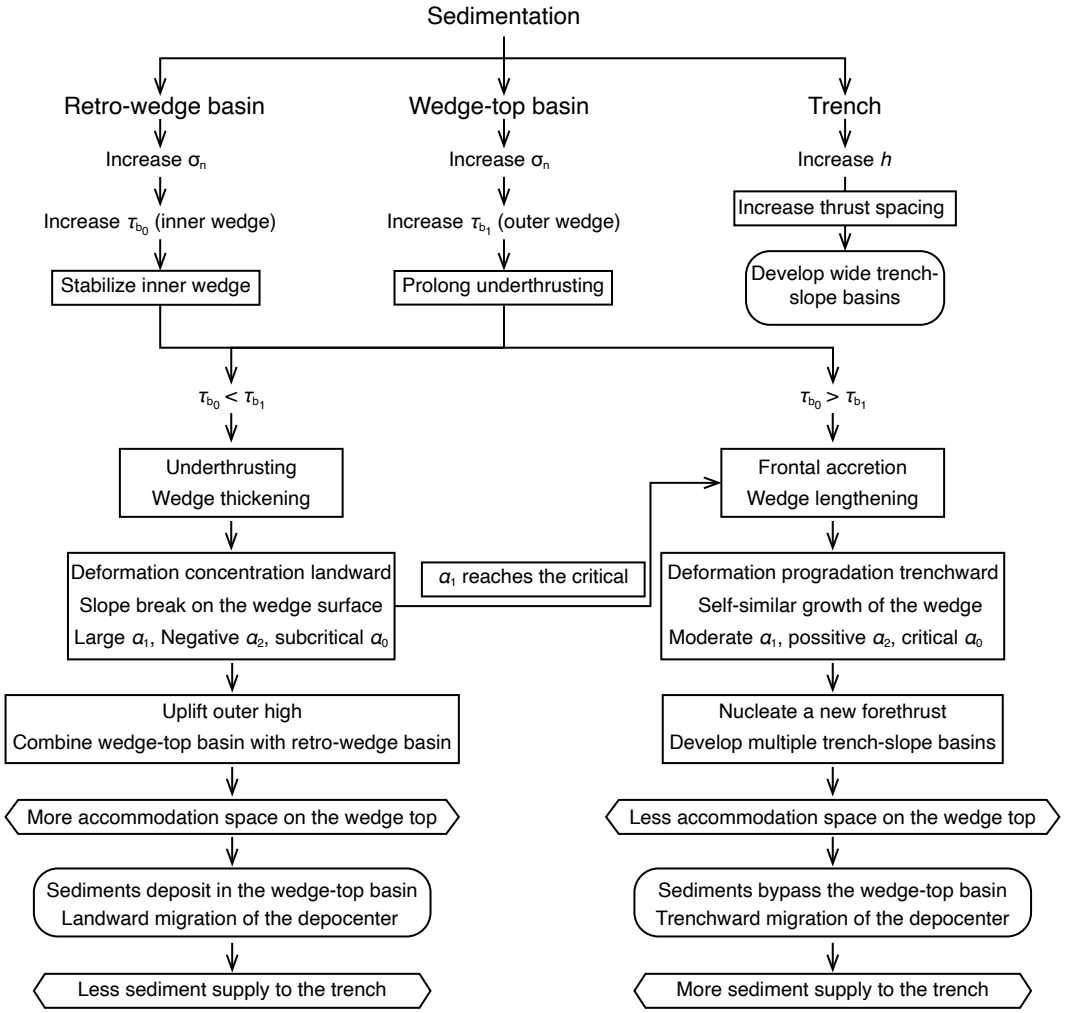

Figure 17. Flow diagram summarizing the interactive relationship between sedimentation (hexagons), wedge deformation (rectangles), and basin evolution (rounded rectangles).

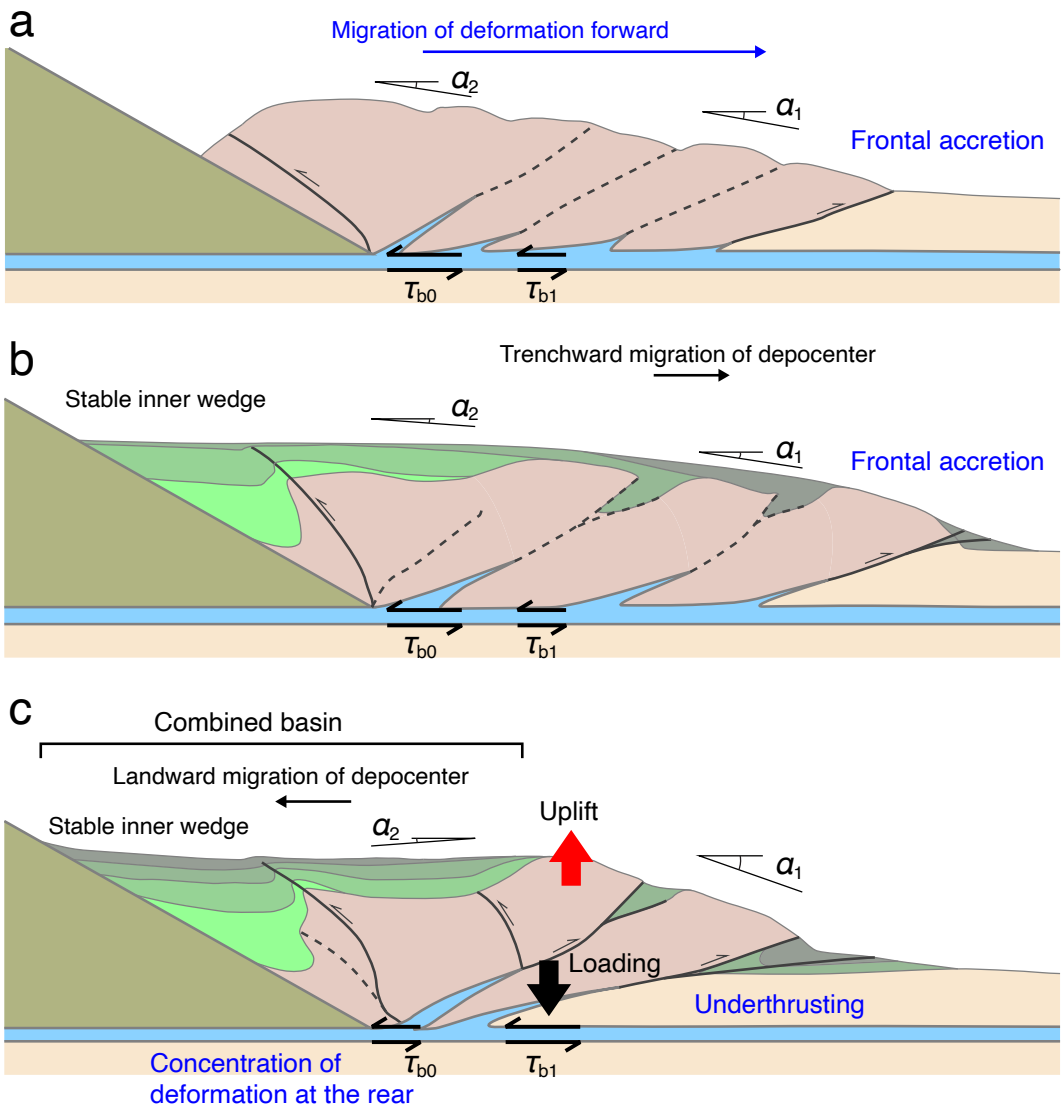

Figure 18. Schematic models of forearc basin formation corresponding to syntectonic sedimentation and accretionary wedge growth. (a) Accretionary wedge without sedimentation. (b) Forward migration of the depocenter in association with progradation of deformation front when the basal resistance on the trenchward side is smaller than on the landward side. (c) Landward migration of the depocenter caused by underthrusting of the incoming layer when the basal coupling at the décollement is stronger than the pre-existing sliding surface.